Boris I. Prilutsky
Donald H. Edwards *Editors*

Neuromechanical Modeling of Posture and Locomotion

Springer

Editors

Boris I. Prilutsky
Georgia Institute of Technology
Atlanta
Georgia
USA

Donald H. Edwards
Georgia State University
Atlanta
Georgia
USA

Chapter 2
A Neuromechanical Model of Spinal Control of Locomotion

Sergey N. Markin, Alexander N. Klishko, Natalia A. Shevtsova, Michel A. Lemay, Boris I. Prilutsky and Ilya A. Rybak

Abstract We have developed a neuromechanical computational model of cat hindlimb locomotion controlled by spinal central pattern generators (CPGs, one per hindlimb) and motion-dependent afferent feedback. Each CPG represents an extension of previously developed two-level model (Rybak et al. J Physiol 577:617–639, 2006a, J Physiol 577:641–658, 2006b) and includes a half-center rhythm generator (RG), generating the locomotor rhythm, and a pattern formation (PF) network operating under control of RG and managing the synergetic activity of different hindlimb motoneuronal pools. The basic two-level CPG model was extended by incorporating additional neural circuits allowing the CPG to generate the complex activity patterns of motoneurons controlling proximal two-joint muscles (Shevtsova et al., Chap. 5, Neuromechanical modeling of posture and locomotion, Springer, New York, 2015). The spinal cord circuitry in the model includes reflex circuits mediating reciprocal inhibition between flexor and extensor motoneurons and disynaptic excitation of extensor motoneurons by load-sensitive afferents. The hindlimbs and trunk were modeled as a 2D system of rigid segments driven by Hill-type muscle actuators with force-length-velocity dependent properties. The musculoskeletal model has been tuned to reproduce the mechanics of locomotion; as a result, the computed motion-dependent activity of muscle group Ia, Ib, and II afferents and the paw-pad cutaneous afferents matched well the cat in vivo afferent recordings reported in the literature (Prilutsky et al., Chap. 10, Neuromechanical modeling of posture and locomotion, Springer, New York, 2015). In the neuromechanical model, the CPG operation is adjusted by afferent feedback from the moving hindlimbs. The

S. N. Markin (✉) · N. A. Shevtsova · I. A. Rybak
Department of Neurobiology and Anatomy, Drexel University College of Medicine,
2900 W. Queen Lane, Philadelphia, PA 19129, USA
e-mail: smarkin@drexelmed.edu

A. N. Klishko · B. I. Prilutsky
School of Applied Physiology, Center for Human Movement Studies,
Georgia Institute of Technology, 555 14th Street NW, Atlanta, GA 30332, USA
e-mail: aklishko3@gatech.edu

M. A. Lemay
Department of Bioengineering, Temple University, 1947 N 12th St, Philadelphia, PA 19122, USA

model demonstrates stable locomotion with realistic mechanical characteristics and exhibits realistic patterns of muscle activity. The model can be used as a testbed to study spinal control of locomotion in various normal and pathological conditions.

Keywords Neuromechanical modeling · Central pattern generator · Afferent feedback · Locomotion · Cat

2.1 Introduction

The mammalian spinal cord contains neural circuits that can generate a basic lo-comotor rhythm in the absence of rhythmic input from higher brain centers and peripheral afferent feedback (Brown 1911; Grillner 1981; Pearson 1995; Rossignol 1996; Orlovsky et al. 1999) These circuits are commonly referred to as the *central pattern generator* (CPG). During normal locomotion, however, the spinal CPG op-erates under the control of afferent feedback and descending signals from supra-spinal centers, which both modify the locomotor pattern generated by the CPG and adjust it to the particular motor task and external environment (Conway et al. 1987; Gossard et al. 1994; Guertin et al. 1995; McCrea et al. 1995; Whelan 1996; Fouad and Pearson 1997; Pearson et al. 1998; Hiebert and Pearson 1999; Orlovsky et al. 1999; Lam and Pearson 2002; Frigon et al. 2010; Gottschall and Nichols 2011). Although the spinal reflexes continue to operate during locomotion, their pathways and relative contribution to motoneuronal activity during locomotion are modified. These modifications range from changes in reflex gain to complete reorganization of reflex pathways and emergence of new reflexes during locomotion (Pearson and Collins 1993; Guertin et al. 1995; McCrea et al. 1995; Pearson 1995; Perreault et al. 1995; Angel et al. 1996; Degtyarenko et al. 1998; Pearson et al. 1998; Burke 1999; Menard et al. 1999; Perreault et al. 1999; Gosgnach et al. 2000; Quevedo et al. 2000; Burke et al. 2001; McCrea 2001; Ross and Nichols 2009; Gottschall and Nichols 2011). An important finding has been that electrical stimulation of the group I extensor afferents enhances extensor activity if delivered during the exten-sor phase of locomotion and resets the rhythm to extension if delivered during the flexor phase (Conway et al. 1987; Guertin et al. 1995). In addition, the influence of the muscle force-sensitive group Ib afferents on ankle extensor activity is reversed from inhibition during non-locomotor conditions to excitation during locomotor activity (Pearson and Collins 1993; Gossard et al. 1994; McCrea et al. 1995), thus providing an additional mechanism for regulation of extensor activity depending on the load on the leg. However, the experiments in spinal cats trained to locomote on a treadmill have shown that these pathways cannot compensate for the total loss of cutaneous feedback from the paw (Bouyer and Rossignol 2003b). The length-dependent afferent feedback from the hip flexors is also important for control of stepping and is involved in the initiation of the swing phase and entrainment of locomotor activity (Andersson and Grillner 1983; Kriellaars et al. 1994; Hiebert et al. 1996; Lam and Pearson 2002).

Despite the significant amount of data on changes in locomotor activity produced by mechanical and electrical stimulations of muscles and neural circuits in the mammalian spinal cord, the structure and operation of spinal locomotor CPG(s) remain unknown (Grillner et al. 2008; McCrea and Rybak 2008; Gossard et al. 2011; Kiehn 2011; Yakovenko 2011; Guertin 2012). Computational models of the mammalian spinal circuitry and musculoskeletal system can complement experimental studies and propose explanations for the complex mechanisms of locomotor pattern generation. Several models of locomotor CPG have been developed based on data from so-called fictive locomotion generated within the spinal cord without afferent feedback from moving limbs (Cohen et al. 1982; Collins and Richmond 1994; Beer et al. 1999; Rybak et al. 2006a). However, as discussed above, afferent signals from moving limbs can reset the locomotor rhythm, advance or delay the phase transitions and modulate the duration of flexor and extensor phases. To understand the contribution of afferent feedback in locomotion, the computational models of spinal circuitries should include afferent feedback from the moving musculoskeletal system. Several such models have been developed and the possible mechanisms for sensory control of the CPG suggested (Taga 1995a, b; Wadden and Ekeberg 1998; Rybak et al. 2002; Ivashko et al. 2003; Ekeberg and Pearson 2005; Maufroy et al. 2008; Aoi et al. 2013; Toth et al. 2013; Nassour et al. 2014); see also Chap. 8 in this book (Aoi 2015). Those models, however, have not attempted to reproduce the locomotor patterns of motoneuronal and afferent activity. Neither have they accurately reproduced the exact kinematics and kinetics of walking.

Our study has focused on the development of a comprehensive neuromechanical model of cat spinal locomotion. The neural subsystem of this model includes a locomotor CPG. The model of this CPG is based on the previously developed two-level model (Rybak et al. 2006a, b). The basic two-level CPG model included separate *rhythm generation* (RG) and *pattern formation* (PF) networks. This basic model has been extended to accommodate and reproduce the realistic activity patterns of motoneurons controlling complex two-joint muscles (see Chap. 5 by Shevtsova et al. 2015). In this study we connected the extended CPG model with the comprehensive hindlimb musculoskeletal model simulating biomechanics of cat walking and providing motion-dependent afferent feedback to the CPG (Prilutsky et al., Chap. 10, in this volume). The combined neuromechanical model demonstrates the ability to generate stable locomotion showing realistic patterns of muscle activity and mechanical characteristics of walking. The model has been used for the investigation of the role of particular afferent pathways for stable walking.

2.2 Musculoskeletal Model of Hindlimbs

The musculoskeletal model of the cat hindlimbs is described in details in Chap. 10 of this book (Prilutsky et al. 2015) and only its brief description is provided here. The two cat's hindlimbs, pelvis and trunk are modeled as a 2D, 10 degrees-of-freedom (DOF) system of rigid segments interconnected by frictionless revolute joints (Fig. 2.1a and b). Interactions of hindlimbs with the ground and the trunk with the forelimbs,
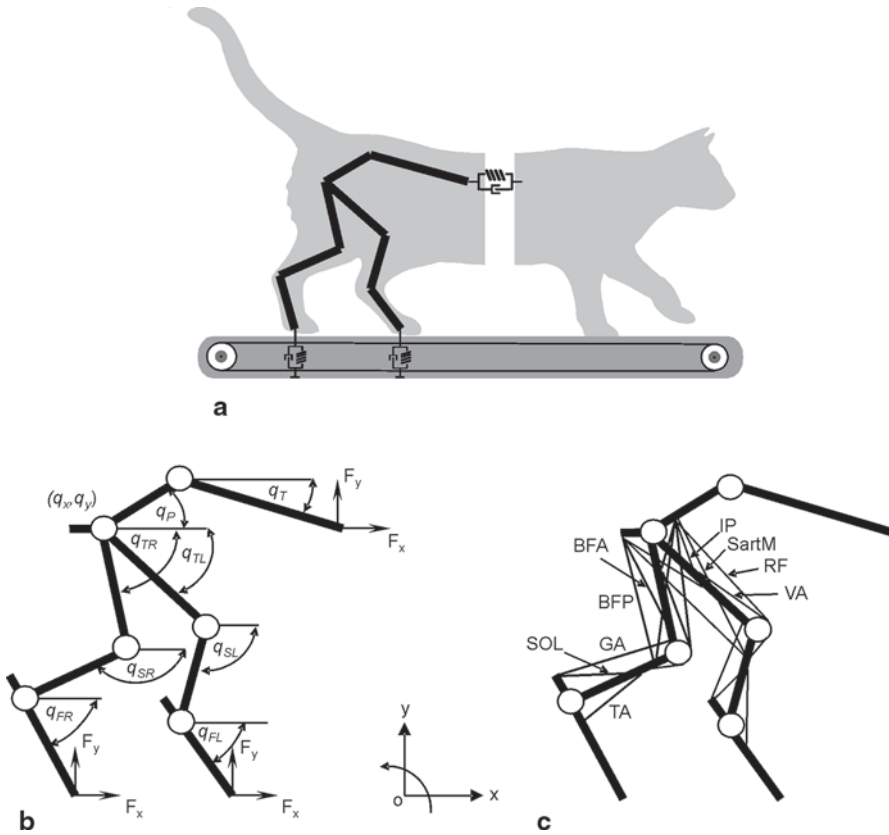
Fig. 2.1 Schematic representation of the musculoskeletal model of the cat hindlimbs and trunk. **a** The hindlimbs and posterior trunk interact with the ground and the anterior trunk and forelimbs. These interactions are modeled as viscoelastic forces. **b** A 10-DOF planar system of rigid segments with frictionless revolute joints representing two hindlimbs, pelvis and posterior trunk. **c** Schematic representation of muscles of the model: *IP* iliopsoas, *BFA* biceps femoris anterior, *RF* rectus femoris, *BFP* biceps femoris posterior, *SartM* sartorius medial, *VA* vastii, *GA* gastrocnemii, *TA* tibialis anterior, and *SOL* soleus. (Adopted from Prilutsky et al., Chap. 10, in this volume)

neck and head are modeled as linear springs with dampers. The inertial parameters of hindlimb segments are computed from the measured mass of the cat and length of each hindlimb segment using the regression equations (Hoy and Zernicke 1985). The equations of motion are derived from the Lagrange equations. The generalized coordinates of the model include the horizontal and vertical positions of the hip and the segment angles (Fig. 2.1b). The equations of hindlimbs dynamics include the vectors of segmental generalized velocities and accelerations, Coriolis and centrifugal forces, gravitational forces, ground and trunk reaction forces, muscle forces, and viscoelastic forces at the joints (for details see Prilutsky et al. 2015, Chap. 10, in this volume).

Each hindlimb in the model is actuated by 9 muscles described by Hill-type models (Fig. 2.1c) with realistic tendon force-length properties, contractile element force-length-velocity properties, muscle mass and angle of pennation as well as a parallel elastic component (Prilutsky et al. 2015; Chap. 10, in this volume). The

description of contractile and activation dynamics of the muscle-tendon actuator can be found in Chap. 10 of this volume (Prilutsky et al. 2015).

Parameters of the musculoskeletal model (constants for the viscoelastic elements producing reaction forces, the tendon slack length, tendon force-length relationship parameters, maximal muscle activation, activation and deactivation time constants for each muscle-tendon unit, etc.; see Prilutsky et al. 2015, Chap. 10, in this volume), were identified by minimizing the mismatch between the simulated and experimentally obtained cat locomotion variables—muscle fascicle lengths/velocities, joint angles, joint moments and ground reaction forces—using a parallel simulated annealing optimization algorithm (Corana et al. 1987). The simulated walking mechanics were obtained by integrating the equations of the limb and muscle dynamics, using the recorded activity of 9 muscles as input and the recorded position and velocity of each generalized hindlimb coordinate at the walking cycle onset as the initial conditions (Prilutsky et al. 2015, Chap. 10, in this volume). The obtained parameters of the musculoskeletal model were within physiological ranges reported in the literature (e.g., Spector et al. 1980; Sacks and Roy 1982; Baratta et al. 1993, 1995; Brown et al. 1996) and allowed for a close match (typically within one standard deviation) between the simulated and recorded joint angles and moments as well as ground reaction forces during walking.

The firing rates of spindle length-sensitive group Ia and II afferents and force-sensitive Golgi tendon organ group Ib afferents are closely correlated with the instantaneous muscle length/stretch velocity and tendon force, respectively, as observed during walking in the cat (Prochazka et al. 1997; Prochazka and Gorassini 1998). This fact makes it possible to estimate the firing rates of spindle and Golgi tendon organ afferents as functions of muscle fascicle length and velocity and tendon force of each muscle-tendon unit in the musculoskeletal model using equations similar to those proposed by Prochazka et al. (Prochazka and Gorassini 1998; Prochazka 1999). Another important afferent signal that indicates the stance phase of locomotion and influences the CPG operation and locomotor rhythm is activity of load-sensitive cutaneous afferents from the paw pad (McCrea 2001). The firing rate of these afferents is computed as the function of the ground reaction force and its time derivative (Prilutsky et al. 2015, Chap. 10, in this volume).

2.3 Model of Spinal Circuitry

2.3.1 Neuron Models

The model of the spinal circuitry in this study represents a modified version of the two-level locomotor CPG model described in Chap. 5 of this volume (Shevtsova et al. 2015). The model includes a bipartite (half-center) rhythm generator, pattern formation network and other interneurons and motoneurons. The interneurons provide basic reflex circuits including reciprocal inhibition of antagonistic motoneurons, recurrent inhibition of motoneurons via Renshaw cells, disynaptic excitation of some motoneuron types, etc. The CPG model of Shevtsova et al. 2015 (see Chap. 5)

was simplified so that each neuronal population was described by an activity-based (non-spiking) neuron model. Two types of neuron models were implemented: one for rhythm-generating RG and PF neurons and motoneurons and the other for all other neurons.

The membrane potentials (V) of principal neurons at RG, PF levels and motoneurons are described by the following equation:

$$C \cdot \frac{dV}{dt} = -I_{NaP} - I_K - I_{Leak} - I_{SynE} - I_{SynI}. \tag{2.1}$$

The membrane potential of all other neurons is described as:

$$C \cdot \frac{dV}{dt} = -I_{Leak} - I_{SynE} - I_{SynI}, \tag{2.2}$$

where C is the neuronal capacitance, I_{Leak} is the leakage current, I_K is potassium rectifier current, I_{NaP} is persistent sodium current; I_{SynE} and I_{SynI} are the excitatory and inhibitory synaptic currents, respectively. The ionic currents are described as follows:

$$
\begin{aligned}
I_{NaP} &= \overline{g}_{NaP} \cdot m_{NaP} \cdot h_{NaP} \cdot (V - E_{Na}); \\
I_K &= \overline{g}_K \cdot m_K^4 \cdot (V - E_K); \\
I_{Leak} &= \overline{g}_{Leak} \cdot (V - E_{Leak}); \\
I_{SynE,i} &= \overline{g}_{SynE} \cdot (V_i - E_{SynE}) \cdot \left(\sum_j a_{ji} \cdot f(V_j) + \sum c_{mi} \cdot d_m + \sum_k w_{ki} \cdot fb_k \right); \\
I_{SynI,i} &= \overline{g}_{SynI} \cdot (V_i - E_{SynI}) \cdot \sum_j b_{ji} \cdot f(V_j),
\end{aligned}
\tag{2.3}
$$

where $\overline{g}_{NaP}$, $\overline{g}_{Leak}$, $\overline{g}_{SynE}$, and $\overline{g}_{SynI}$ are the maximal conductances of the corresponding ionic channels; E_{Na}, E_K, E_L, E_{SynE}, and E_{SynI} are the corresponding reversal potentials; a_{ji} defines the weight of the excitatory synaptic input from neuron j to neuron i; b_{ji} defines the weight of the inhibitory input from neuron j to neuron i; c_{mi} defines the weight of the excitatory drive d_m to neuron i; w_{ki} defines the synaptic weight of afferent feedback fb_k ($k=$Ia, Ib, II, cutaneous) to neuron i; (see Tables 2.1, 2.2, 2.3, 2.4, 2.5, 2.6, 2.7, 2.8, and 2.9 in Appendix). Activation of the potassium delayed rectifier and persistent sodium currents is considered instantaneous. Voltage dependent activation and inactivation variables and time constant for the potassium delayed rectifier and persistent sodium channels are described as follows:

$$
\begin{aligned}
m_K &= 1 / (1 + \exp(-(V + 44.5) / 5)), \\
m_{NaP} &= 1 / (1 + \exp(-(V + 47.1) / 3.1)), \\
\tau_{hNaP} \cdot \frac{d}{dt} h_{NaP} &= h_{\infty NaP} - h_{NaP}, \\
h_{\infty NaP} &= 1 / (1 + \exp((V + 51) / 4)), \\
\tau_{hNaP} &= \tau_{hNaP\max} / \cosh((V + 51) / 8).
\end{aligned}
\tag{2.4}
$$

The neuron output activity is defined by a nonlinear function $f(V)$:

$$f(V) = \begin{cases} 1/(1+\exp\ (-(V-V_{1/2})/k)), & if\ \ V \geq V_{tr}; \\ 0, & if\ \ \ V < V_{tr}, \end{cases}$$ (2.5)

where $V_{1/2}$ is the half-activation voltage, k defines the slope of the output function and V_{tr} is the threshold.

The following values of neuronal parameters were used: $C = 20$ pF; $E_{Na} = 55$ mV, $E_{K} = -80$ mV, $E_{SynE} = -10$ mV, $E_{SynI} = -70$ mV, $E_{Leak} = -64$ mV for RG, PF neurons and motoneurons and -60 mV for all other neurons; $\bar{g}_{K} = 4.5$ nS, $\bar{g}_{Leak} = 1.60$ nS, $\bar{g}_{SynE} = \bar{g}_{SynI} = 10.0$ nS, $\bar{g}_{NaP} = 3.5$ nS for RG neurons, 0.5 nS for PF neurons, and 0.3 nS for motoneurons; $\tau_{hNaP} = 600$ ms. Parameters of $f(V)$ function were $V_{1/2} = -30$ mV, $V_{tr} = -50$ mV, $k = 3$ mV for motoneurons and 8 mV for other neurons.

The model of locomotor center (Fig. 2.2) incorporates the model of CPG and basic reflex circuits mediating the reciprocal inhibition of antagonistic motoneurons via Ia inhibitory interneurons, recurrent inhibition of motoneurons via Renshaw cells (RC), non-reciprocal motoneuron inhibition (Ib cells) and disynaptic excitation of extensor motoneurons (Ia and Ib cells) (Fig. 2.3).

The conceptual architecture of the CPG model is based on the idea of a two-level locomotor CPG (Rybak et al. 2006a, b; McCrea and Rybak 2007, 2008). According to this hypothesis, the locomotor CPG consists of a half-center rhythm generator and multiple pattern formation circuits controlling different synergist and antagonist motoneuron pools (see Figs. 2.2 and 2.3). Depending on the input from the RG and the interactions within the PF network, each PF neuron is active within the particular phase(s) of the locomotor cycle and produces a phase-specific activity pattern. The specific principal PF elements control the corresponding group of synergistic motoneurons that are active synchronously. Organization of multiple neural circuits that control the activation of synergistic motoneuron groups is mainly unknown. Previous analysis based on the onset and offset times in motoneuron/muscle activity allowed to identify several synergistic groups of motoneurons operating during locomotion (Markin et al. 2012). The identified groups (see Fig. 2.4) include hip flexors (IP, SartM), hip extensor (BFA), knee extensor (VA), ankle flexor (TA), ankle extensors (GA, SOL), and two two-joint muscles BFP and RF, which demonstrate activity in both swing and stance phases. Figure 2.5 shows the proposed organization of rhythm generator and pattern formation circuits in the CPG controlling one hindlimb. All PF circuits receive excitatory and inhibitory inputs from rhythm generator and control flexor and extensor motoneurons operating at hip, knee and ankle as well as motoneurons controlling two-joint muscles (BFP, RF). Each joint-related PF circuitry is a half-center network consisting of PF-F and PF-E neurons reciprocally inhibiting each other via Inpf-F and Inpf-E inhibitory interneurons, respectively. The detailing description of PF organization can be found in Chap. 5 of this volume (Shevtsova et al. 2015).
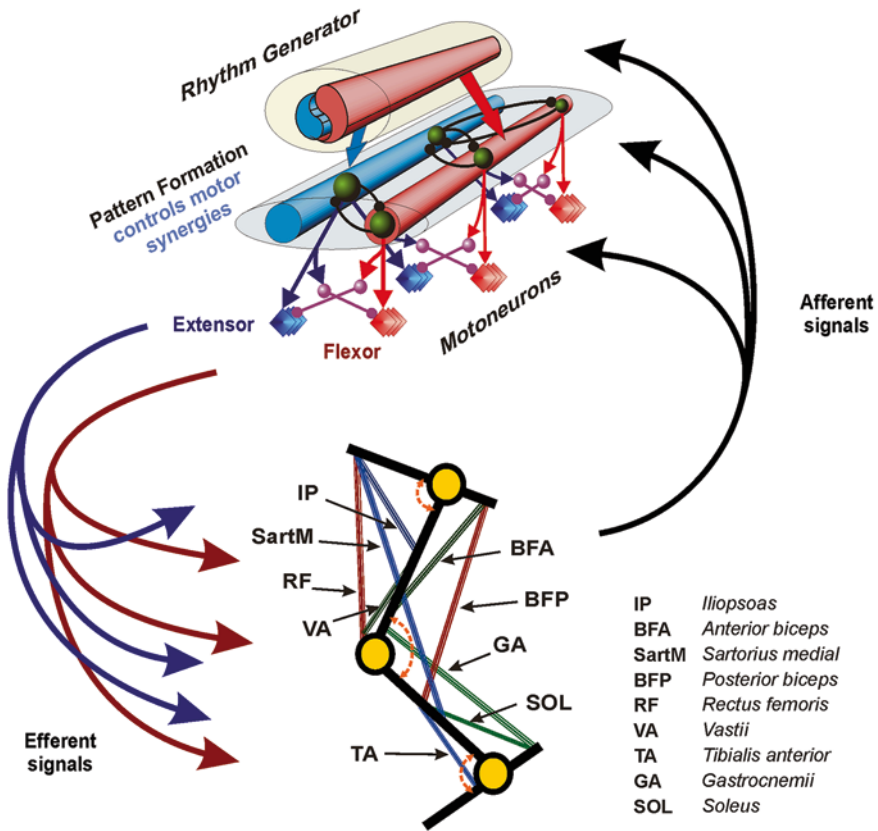
Fig. 2.2 General schematics of the neuromechanical model of the cat hindlimb locomotor control. The neural part of the model consists of the two-level locomotor CPG that controls the hindlimb musculoskeletal model. The activity of corresponding motoneuron pools controls major hindlimb muscles that drive the 10-DOF cat hindlimb model. The generated somatosensory feedback signals from the moving musculoskeletal hindlimb model (i.e., firing rates of group I and II muscle and paw pad cutaneous afferents) project onto both levels of the CPG (*RG* rhythm generator and *PF* pattern formation) and motoneuron level as well

2.4   Control of CPG by Afferent Feedback

Although the locomotor CPG can generate rhythm in the absence of sensory feedback signals, the sensory feedback plays a critical role in regulating phase transitions, stabilizing locomotor movements, contributing to weight support during the stance phase, and adjusting the locomotor pattern to the constantly changing external environment. A possible organization of afferent pathways to the CPG for a simple 1-DOF musculoskeletal system has been recently proposed (Markin et al. 2010). According to this organization, the stance-swing (extensor-flexor) phase transition was controlled by both the reduction of force-dependent afferent activity from the
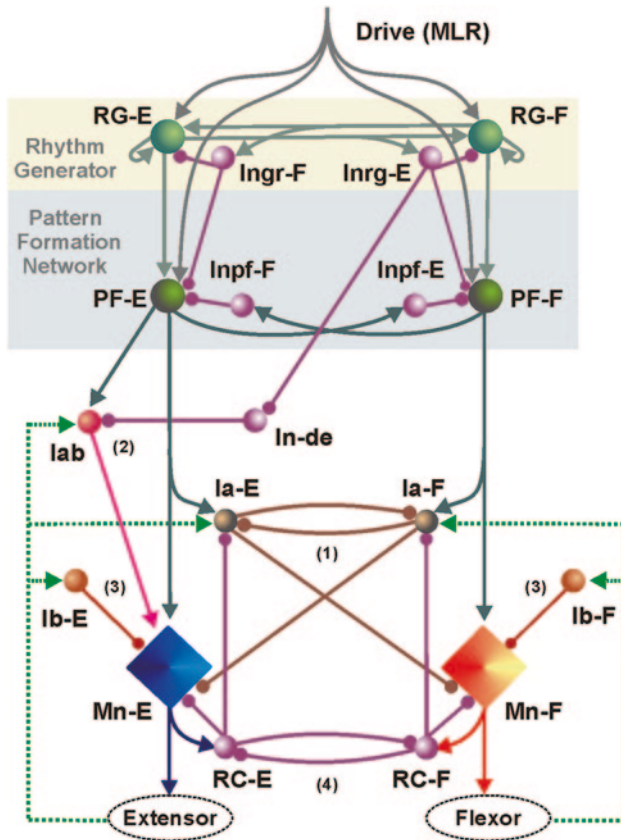
Fig. 2.3 Basic model of the two-level locomotor CPG model by (Rybak et al. 2006a, b) including reflex circuits: *1* reciprocal inhibition of antagonistic motoneurons via Ia inhibitory interneurons (*Ia-E* and *Ia-F*, correspondingly), *2* disynaptic excitation of extensor muscle motoneurons via Iab interneurons, *3* non-reciprocal inhibition of motoneurons via Ib inhibitory interneurons, and *4* recurrent inhibition via Renshaw cells (*RC-E* and *RC-F*, respectively)

extensor muscles and the increase in length-dependent afferent activity from the flexor muscles. Because of this organization, the duration of the stance phase depended on the locomotor speed. In contrast, the timing of the swing-stance (flexor-extensor) phase transition was mainly controlled by the length/velocity-dependent afferent activity from the hip extensor muscles; this feedback signal adjusted the duration of the flexor phase to limb kinematics during the swing phase, keeping the swing duration relatively constant.

In the present, more realistic neuromechanical model we have adopted the organization of sensory pathways between muscle afferents and RG-interneurons from the previous work (Markin et al. 2010). The type and organization of afferent pathways from the moving musculoskeletal system to the CPG have been chosen based
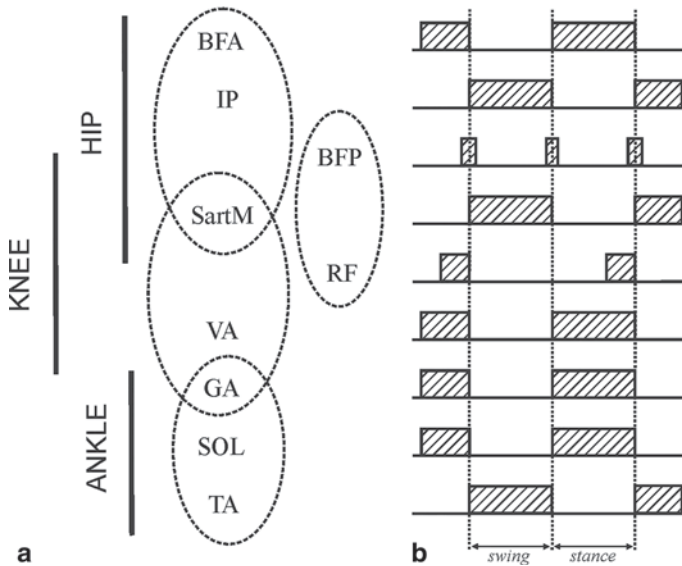
Fig. 2.4 Phases of activity of cat hindlimb muscles during real locomotion. **a** The possible organization of synergist motoneuron groups at the pattern formation level. Three circuits at the pattern formation level (hip-PF, knee-PF and ankle-PF) are introduced to control motoneuron groups innervating joint specific muscles: (1) BFA, IP, SartM as hip muscles; (2) VA, SartM, GA as knee muscles; and (3) GA, SOL, TA as ankle muscles. Note that two two-joint muscles (SartM and GA) receive control signal from hip-PF/knee-PF and knee-PF/ankle-PF sub-networks, respectively. The fourth circuit at pattern formation level specifically controls BFP and RF muscles that are partially active during both flexor and extensor phases. **b** Schematic representation of periods of EMG activity during level walking in the cat. While most of the hindlimb muscles are active during most of swing (flexor) or stance (extensor) phases, the two-joint BFP and RF muscles are only active at the swing-stance or stance-swing phase transition (BFP) or in the later part of the stance phase (RF)

on the following experimental data: (1) muscle length-sensitive spindle afferents of hip extensor and flexor muscles influence the flexor-extensor and extensor-flexor phase transitions (Perreault et al. 1995; Lam and Pearson 2002; McVea et al. 2005); and (2) activation of both group I and II afferents of ankle flexors can terminate flexor and initiate extensor phases during fictive locomotion (Perreault et al. 1995; Stecina et al. 2005); (3) group Ib afferents from the Golgi tendons organs of ankle extensors are responsible for prolongation of the stance phase (Duysens and Pearson 1980; Pearson 2008); (4) stimulation of cutaneous afferents innervating the paw pad can prolong the stance phase and is responsible for terminating the ongoing swing and initiating the stance phase (McCrea 2001; Rossignol et al. 2006). A possible organization of afferent signals at the RG-level for the CPG model is presented in Fig. 2.6. Two additional interneurons (Frg-F and Frg-E) are incorporated into the CPG model. These neurons receive the multi-modal afferent input signals from the afferents listed above and project their excitatory activity onto the corresponding neurons at the RG level.
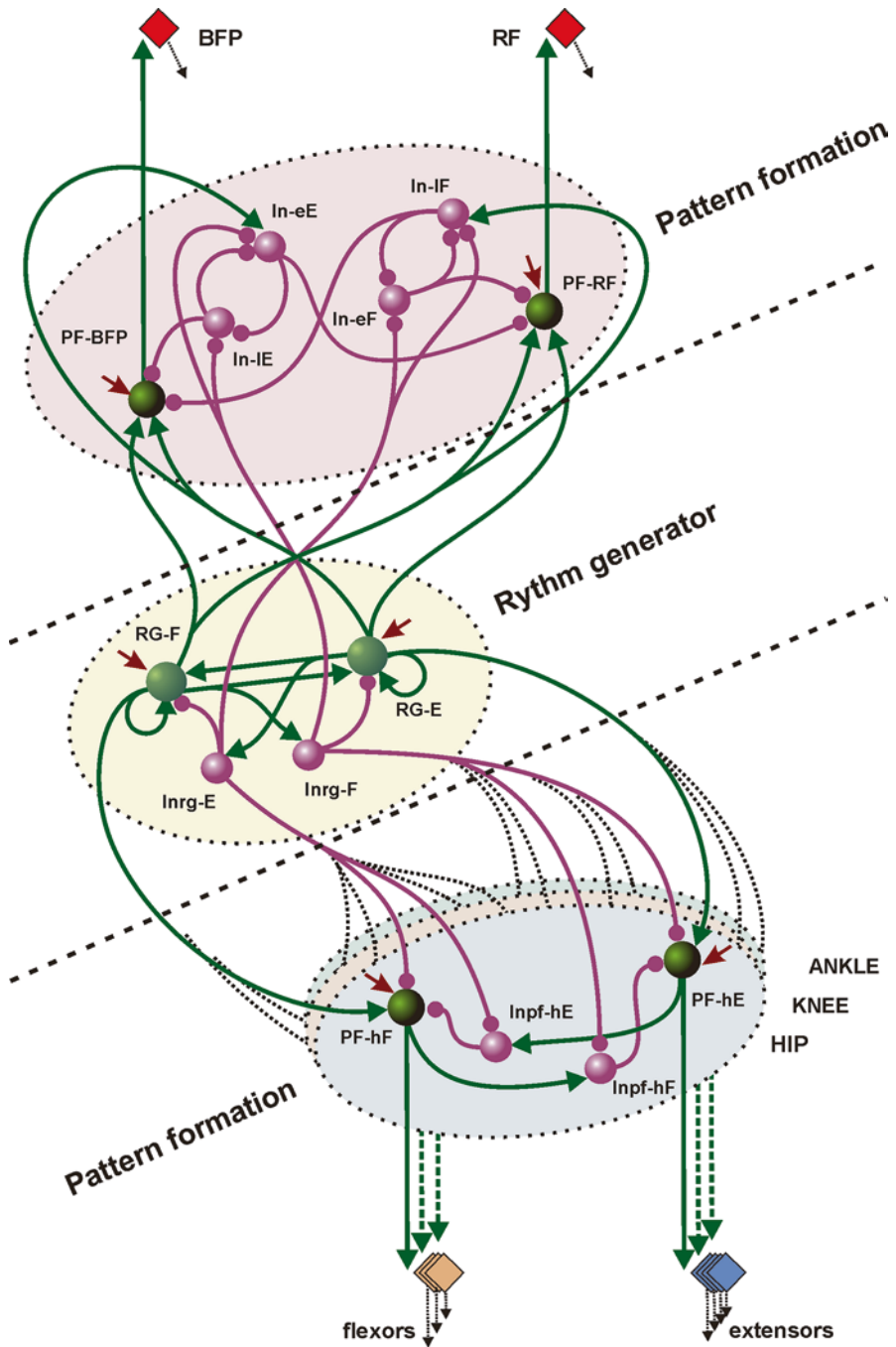
Fig. 2.5 A general diagram of the comprehensive model of locomotor circuitry. The rhythm generator (in the *center* of the figure) mediates rhythmic excitatory and inhibitory drive to the three pattern formation networks that control distinct synergistic motoneuron groups innervating mus-
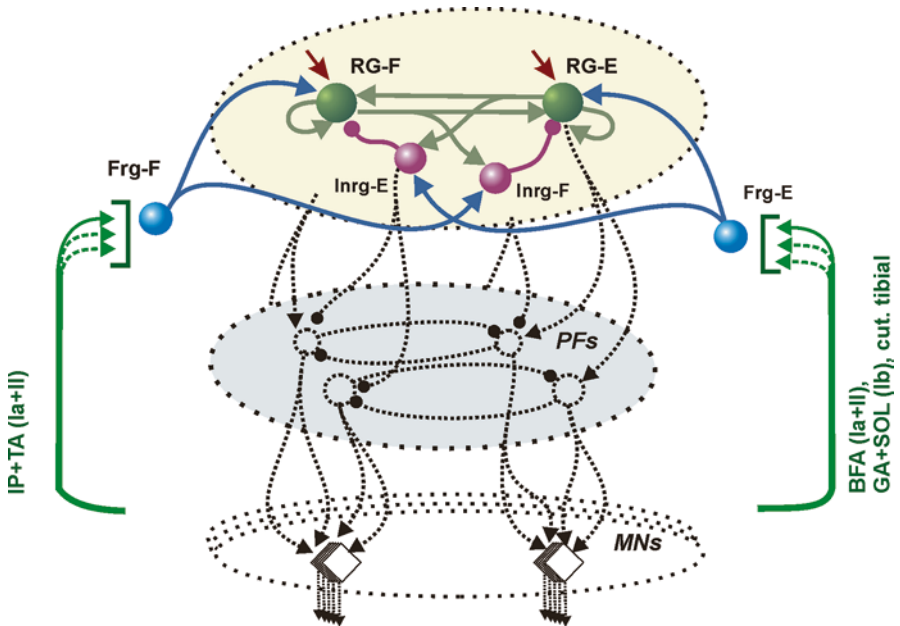
Fig. 2.6 Organization of afferent feedback projections onto the rhythm generator *(RG)*. Two additional interneurons (Frg-F and Frg-E) receive proprioceptive feedback signals from hip and ankle muscles and cutaneous paw pad afferents and distribute them between flexor and extensor parts of the rhythm generator. Specifically, Frg-F neuron receives excitatory inputs from IP-Ia, IP-II, TA-Ia, TA-II afferents and mediates the excitation to the flexor part of the rhythm generator (RG-F and Inrg-F, respectively); afferent feedback signals from the BFA-Ia, BFA-II, GA-Ib, SOL-Ib and cutaneous paw pad afferents converge to and excite the extensor half-center of the rhythm generator (RG-E and Inrg-E, respectively) via Frg-E. Weights of synaptic connections between afferent feedback signals and the corresponding interneurons at the RG level are given in Tables 2.1 and 2.9 in Appendix

In the current two-level CPG architecture, the PF networks are interposed between the RG and motoneurons. Each PF-neuron is active during a particular phase of the walking cycle and produces a phase-specific synchronized activation of the corresponding group of synergetic motoneuron pools. We hypothesized that each principal PF neuron (hip-PF, knee-PF, ankle-PF and BFP-RF-PF) receives proprioceptive feedback from the group of synergetic muscles that are regulated by this neuron. The schematic of afferent pathways based on this approach is presented in

---

cles of individual joints (*lower* part of the figure) and a pattern formation network that controls the two separate motoneuron groups innervating two-joint *BFP* and *RF* muscles (*upper* part of the figure). Here and further in the figures, the inhibitory and excitatory connections are shown as *solid circles* and *arrows*, respectively; *red arrows* indicate supra-spinal tonic drive. Weights of synaptic connections within locomotor CPG circuitry are given in Tables 2.1–2.5 in Appendix
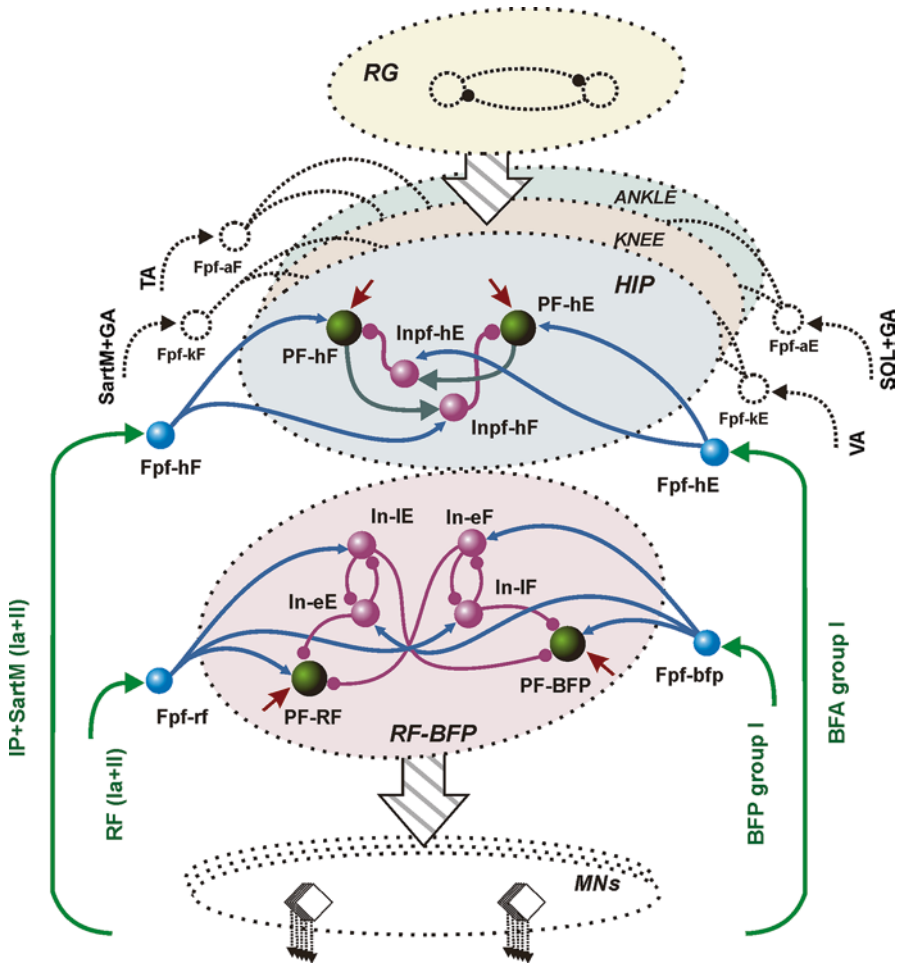
Fig. 2.7 Organization of afferent feedback signals projected onto the pattern formation *(PF)* networks. Eight interneurons (Fpf-hE, Fpf-hF, Fpf-kE, Fpf-kF, Fpf-aE, Fpf-aF, Fpf-rf and Fpf-bfp) receive afferent signals from the musculoskeletal system and excite the corresponding interneurons at the pattern formation level. Tables 2.2–2.5 and 2.9 in Appendix provide additional information about weights of synaptic connections between afferent signals and correspondent interneurons of locomotor CPG at the PF level

Fig. 2.7. Eight additional neurons at the PF-level (Fpf-hE, Fpf-hF, Fpf-kE, Fpf-kF, Fpf-aE, Fpf-aF, Fpf-rf and Fpf-bfp) receive proprioceptive feedback from the corresponding muscles and distribute the excitatory signal among interneurons within the particular PF neurons that control muscles belonging to the same muscle synergy. The flexor part of each joint-specific PF sub-network receives input from groups Ia and II spindle afferents of the corresponding muscles, whereas the extensor half-centers receive afferent input from group I afferents (Ia and Ib) of the corresponding

muscles. Thus, the Fpf-hE and Fpf-hF neurons receive afferent signals from hip extensor (BFA) and hip flexors (IP and SartM), respectively. These neurons mediate excitatory inputs to the PF-hE, PF-hF, Inpf-hE and Inpf-hF neurons, which in turn control the activity of BFA, IP and SartM interneurons. The Fpf-kE and Fpf-kF neurons, that receive proprioceptive input from knee flexors (SartM and GA) and knee extensor (VA) afferents, distribute the excitatory signals within the knee-specific PF sub-network. The knee-PF neuron controls only knee related motoneuron group (SartM, GA and VA). The ankle-PF circuitry that controls ankle related muscles (GA, SOL and TA) receives excitatory input from the Fpf-aE and Fpf-aF neurons, which operate under proprioceptive control from GA, SOL and TA muscles. Note, the motoneurons that control the two-joint SartM and GA muscles (spanning hip/ knee and knee/ankle, respectively), receive inputs from the corresponding PF-circuits. Specifically, the SartM motoneuron receives excitatory signals from the hip and knee PF sub-networks (both inputs are from the flexor parts of the corresponding PF circuitry), and the GA motoneuron is controlled by the knee and ankle PF sub-networks (one input form the flexor part of the knee-specific PF circuitry and the other input from the extensor part of the ankle-specific PF circuitry). The BFP and RF muscles that also span two joints (hip and knee) are active either during the stance-swing and swing-stance phase transitions (BFP) or during the late stance (RF). These two motoneuron pools are controlled by the distinct PF network (RF-BFP circuitry) whose activity is modulated by the corresponding feedback inputs from RF and BPF muscles only (Fig. 2.7).

2.5   Organization of Spinal Autogenic and Heterogenic Reflex Pathways

Besides the CPG circuits the neural sub-system in the model contains reflex circuits and pathways that allow the motoneurons to receive afferent feedback input from the muscles they innervate (autogenic pathways) and from other muscles (heterogenic pathways) or skin afferents (see also Chap. 3 in this volume by Nichols et al. 2015). These pathways and circuits provide: (1) disynaptic excitation of extensors by group I extensor afferents during extensor phase of locomotion (Angel et al. 1996; Rybak et al. 2006b); (2) excitation of extensors via load-sensitive paw pad cutaneous afferents (McCrea 2001; Bouyer and Rossignol 2003b); (3) recurrent inhibition of motoneurons via Renshaw cells (McCrea et al. 1980; Nishimaru et al. 2006); (4) Ia-evoked monosynaptic excitation of homonymous and synergist motoneuron pools (Eccles et al. 1957a; Eccles and Lundberg 1958; Nichols et al. 1999, 2015); (5) the reciprocal disynaptic inhibition of antagonistic motoneuron pools via the Ia inhibitory interneurons (Feldman and Orlovsky 1975; Pratt and Jordan 1987); and (6) non-reciprocal Ib inhibition of synergist motoneuron pools (Eccles et al. 1957b; Nichols et al. 1999, 2015).
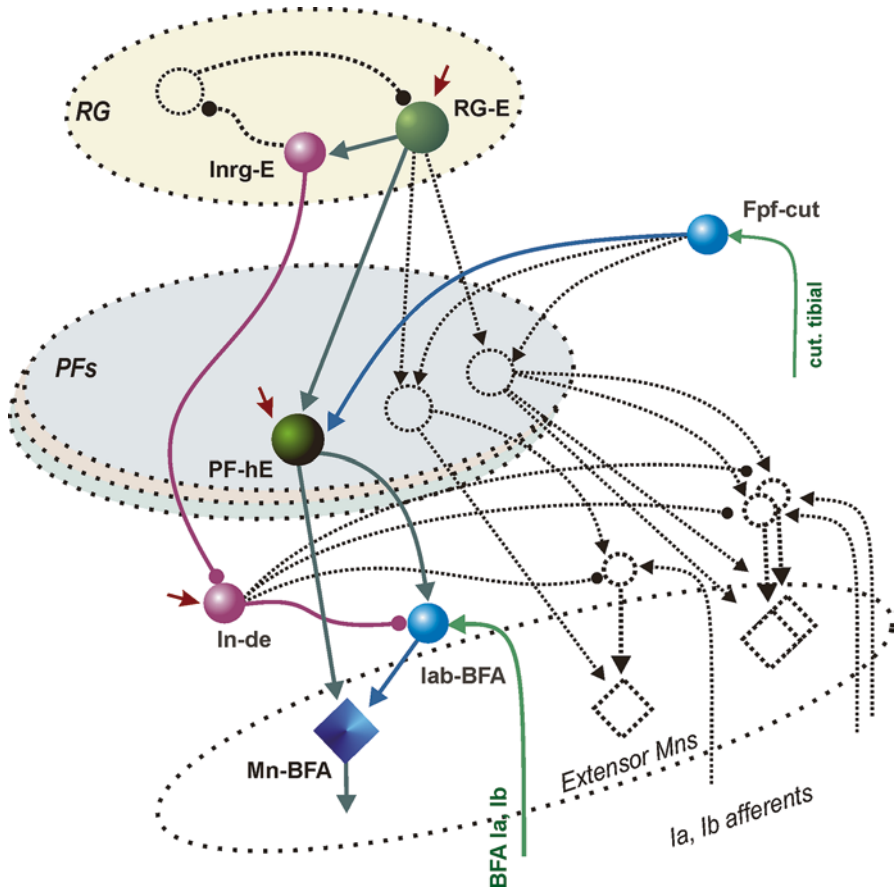
Fig. 2.8 Organization of the disynaptic excitation of extensor motoneurons during the extensor phase of locomotion. The Iab-BFA interneuron provides phase-dependent disynaptic excitation of extensor motoneuron (Mn-BFA) by extensor group I afferents. During the stance phase of locomotion, Iab-BFA interneuron is released from inhibition by the In-de interneuron and receives additional excitatory signal from the PF-hE at the PF level. The hypothetical Fpf-cut interneuron receives signals from cutaneous paw pad afferents and mediates additional excitation on extensor parts of the joint-specific PF circuitry. (see Table 2.6 in Appendix)

2.5.1 Disynaptic Excitation of Extensor Motoneurons by Group I Extensor and Cutaneous Paw Pad Afferents

An important function of proprioceptive feedback during locomotion is to reinforce ongoing motor activity during stance (Pearson 1995). One of the mechanisms of reinforcement of ongoing extensors activity is additional disynaptic excitatory input from group I afferents of extensor muscles. Disynaptic excitation of extensor motoneurons was demonstrated in fictive locomotion when during the extensor phase extensor afferents were electrically stimulated at group I strength (McCrea et al. 1995; Angel et al. 1996; Degtyarenko et al. 1998). Figure 2.8 shows the or-

ganization of additional circuitry that provides the disynaptic reflex excitation to extensor motoneurons (Rybak et al. 2006a, b). Four additional excitatory neurons (Iab-BFA, Iab-VA, Iab-GA and Iab-SOL) providing disynaptic excitation to extensor motoneurons (BFA, VA, GA, SOL) have been included in the neural circuitry of the model (see Fig. 2.8). These neurons are inhibited during the swing phase due to inhibitory input from the hypothetical In-de neuron that in turn receives inhibitory input from the Inrg-E interneuron. During the stance phase of locomotion (i.e., when the Inrg-E inhibitory interneuron is active), the In-de neuron is inhibited and thereby the Iab-BFA, Iab-VA, Iab-GA and Iab-SOL neurons can be activated by both excitatory inputs from appropriate interneurons at the pattern formation level and group I afferent feedback from the corresponding muscles.

The cutaneous afferents from the paw pad can also play a crucial role in weight support during locomotion (Bouyer and Rossignol 2003a, b). Therefore, we have incorporated in the model additional afferent pathways originating from the cutaneous paw pad afferents (Fig. 2.8). They are mediated by the Fpf-cut interneuron and contribute to weight support. The Fpf-cut neuron receives input from cutaneous paw pad afferents and excites the principal neurons at the pattern formation level (namely, PF-hE, PF-kE and PF-aE), which activate BFA (hip extensors), VA (knee extensors), GA and SOL (ankle extensors) muscles.

2.5.2   Recurrent Inhibition via Renshaw Cells

The activity of motoneurons is also regulated by Renshaw cells. These interneurons fire rhythmically during locomotion and produce feedback inhibition to homonymous and synergetic motoneurons (McCrea et al. 1980; Pratt and Jordan 1987). They also regulate the activity of interneurons which provide Ia reciprocal inhibition (Jankowska 1992; Alvarez and Fyffe 2007). Interestingly, Renshaw cells receive rhythmic inhibitory inputs in both the active and silent phases during fictive locomotion (Nishimaru et al. 2006). It has been shown that Renshaw cells can receive inhibition from Renshaw cells excited by antagonist motoneuron pools (Ryall 1970; Windhorst 1996), which may explain the inhibition of Renshaw cells in the non-active phase but not in the active phase. One of the possible sources of this inhibition could be ipsilateral populations of interneurons of locomotor circuitry (Nishimaru et al. 2006). The implementation of a possible connectivity for Renshaw cells in the model is presented in Fig. 2.9.

2.5.3   Other Reflexes

In the cat, activation of group Ia muscle spindle afferents evokes the stretch reflex, a monosynaptic excitation of synergist motoneurons with disynaptic inhibition of antagonist motoneurons mediated by Ia inhibitory interneurons (Eccles et al. 1956;

Fig. 2.9 Possible organization of interconnections between Renshaw cells *(RC)*, motoneurons *(MN)* and other interneurons in the locomotor CPG. Renshaw cells receive excitatory input from particular motoneurons and inhibit the same and the synergist motoneurons. Renshaw cells also provide inhibitory signals to Ia interneurons and receive the ipsilateral inhibition from CPG circuitry and Renshaw cell of the antagonist motoneurons. Here and further the unlabeled *green circle* represents a principal interneuron at PF level that controls a corresponding motoneuron; the unlabeled *purple circle* inside the PF level represents inhibitory interneuron at the PF level that receives excitatory input from corresponding principal interneuron. (see Tables 2.2–2.5, and 2.7 in Appendix for details)

Baldissera et al. 1981; Jankowska 1992). A simplified scheme of the monosynaptic stretch reflex with disynaptic Ia reciprocal inhibition circuitry is shown in Fig. 2.10a. The additional Ia interneurons which receive Ia afferent input and mediate inhibition to antagonist motoneurons are introduced for the following pairs of antagonist muscles: IP/BFA, SartM/RF, SartM/VA, RF/BFP, BFP/VA, GA/RF, GA/VA, GA/TA, SOL/TA (Lloyd 1946; Eccles and Lundberg 1958). These interneurons also receive mutual inhibition from the antagonist Ia interneurons and the inhibitory input from the Renshaw cells (RC) coupled with the corresponding synergist motoneurons (Jankowska 1992).

Monosynaptic excitation via Ia afferent feedback has been implemented for all motoneurons of the locomotor spinal circuitry (Fig. 2.10a). To simulate the tonic presynaptic depression of Ia monosynaptic excitation of motoneurons occurring during locomotion (Gosgnach et al. 2000), the weights of monosynaptic excitatory inputs of Ia afferents to the corresponding motoneurons have been set to be relatively small values.

Fig. 2.10 General schematic of basic reflexes implemented in the model of the locomotor circuitry (for further details see Table 2.7 in Appendix). **a** Monosynaptic stretch reflex *(1)* and Ia-reciprocal inhibition (*2*) pathways. The Ia interneuron is excited by the primary muscle spindle afferents from the corresponding muscle, and mediates Ia reciprocal inhibition of antagonist motoneurons (see (Jankowska 1992)). **b** Non-reciprocal inhibition circuitry. The Ib⁻ inhibitory interneuron receives the excitatory input from Ib afferents of a muscle and inhibits the motoneurons innervating the corresponding muscle and its synergists (Jami 1992). **c** Force-dependent excitation between motoneurons innervating a two-joint muscle and its one-joint antagonist (e.g., from GA to TA) has been postulated based on a biomechanical analysis of muscle coordination (Prilutsky 2000). Such force-dependent excitation has been observed during muscle stretch evoked responses in the decerebrate cat. (Nichols et al. 2015)

Activation of Golgi tendon organ Ib afferents evokes a short latency inhibition of synergist motoneurons (Jami 1992; Jankowska 1992; Nichols et al. 1999). The principal circuitry that *provides non-reciprocal inhibition* of motoneurons is shown in Fig. 2.10b. This schematic is based on the circuitry described previously in (Rybak et al. 2006a, b). We introduced the additional Ib⁻ interneuron that receives an excitatory Ib feedback from the corresponding muscle and an excitatory signal from interneurons at the pattern formation level. Because Ib inhibition is enhanced in decerebrate animals compared to intact animals (Whelan and Pearson 1997), we suggested an additional interneuron (In-nr) that might receive excitatory supra-spinal signals and mediate inhibitory signal on Ib⁻ interneuron. The In-nr interneuron can be used to modulate activity of the corresponding motoneuron pool during execution of specific locomotor tasks. The Ib⁻ interneuron relays the inhibitory signal to the same motoneuron and motoneurons innervating the synergists: BFP→(BFA, SartM), RF→(IP, VA), GA→(BFP, SartM, SOL).

A *force-dependent excitation* (Fig. 2.10c) is somewhat opposite to non-reciprocal inhibition. It is mediated by Ib afferents from two-joint muscles to their one-joint antagonists (e.g., from GA to TA). The force-dependent excitation has been postulated based on a biomechanical analysis of muscle coordination (Prilutsky 2000). Such force-dependent excitation has been observed during muscle stretch evoked responses in the decerebrate cat (Nichols et al. 2015).

2.5.4 Left-Right Hindlimb Coordination

The neuromechanical computational model of the locomotor circuitry has been constructed using the hypothesis that each hindlimb is controlled by a single CPG (Orlovsky et al. 1999), and the two hindlimb CPGs are connected via a coordinating neural network. The interaction between the left and right parts of the locomotor circuitry controlling the two hindlimbs is implemented via several excitatory and inhibitory populations of so-called *commissural interneurons* (CINs) relaying coordinating signals between the left and right CPGs. These interneuron populations project their connections onto the contralateral side of the spinal cord and coordinate operation of the contralateral CPG (Butt and Kiehn 2003; Lanuza et al. 2004; Jankowska et al. 2009; Zhong et al. 2012; Rybak et al. 2013). The inhibitory CINs mediate mutual inhibition between the ipsi- and contra-lateral CPGs and provide the alternation in activation of left and right homonymous CPG half-centers during normal walking. The excitatory CINs may provide direct excitation of the contralateral CPG, promoting synchronization between the homonymous CPG half-centers (as in the case of hopping or galloping), or contribute to mutual inhibition and alternation by acting via inhibitory interneurons located on each side. Because this chapter is focusing on normal walking we consider the possible organization of circuitry between CINs and contra-lateral CPG which provides alternating activity between left and right hindlimbs. In addition, according to recent experimental data obtained by (Jankowska et al. 2009), commissural interneurons (both excitatory and inhibi-
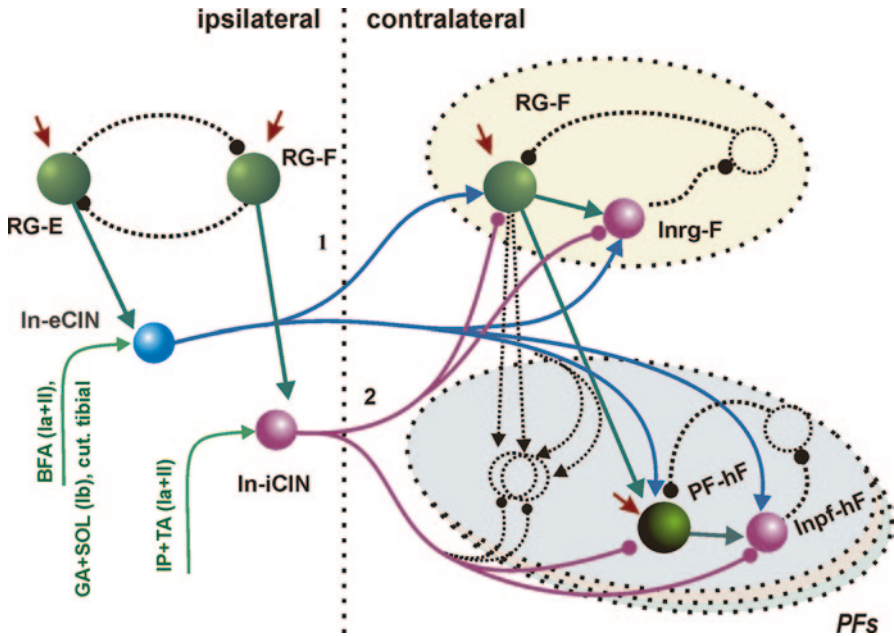
Fig. 2.11 Possible connectivity between commissural interneurons and neurons of the contralateral locomotor circuitry. Two pathways providing alternation between *left* and *right* limbs during normal walking are presented in the figure: **1** excitatory pathways from the excitatory neuron *In-eCIN* that project excitation to the interneurons of the flexor part of the contra-lateral CPG (*blue* pathways); **2** inhibitory pathways from the inhibitory neuron *In-iCIN* to the interneurons at the *RG* and *PF* levels of the contra-lateral CPG (*purple* pathways). Tables 2.8 and 2.9 in Appendix provide additional information about weights of synaptic connections within *left-right* coordination circuitry

tory) receive afferent feedback from group I and/or group II afferents from a number of muscles including *quadriceps, sartorius medial, biceps femoris posterior* and *semitendinosus, biceps femoris anterior* and *semimembranosus, gastrocnemius* and *soleus, plantaris, flexor digitorum* and *hallucis longus*, and *deep peroneal* muscles.

Based on the above information, we propose the general schematic of circuitry providing left-right coordination between the corresponding hindlimbs (Fig. 2.11). Two types of CIN neurons (excitatory and inhibitory; In-eCIN and In-iCIN, respectively) were introduced to the locomotor circuitry model. The excitatory signals from the ipsilateral interneurons at the rhythm generator level (RG-E and RG-F) project their action to the flexor part of the contralateral CPG (see Fig. 2.11). They also receive monosynaptic multi-modal afferent input from muscles such as: IP and TA (Ia + II) to In-iCIN; BFA (Ia + II) and GA + SOL (Ib) to In-eCIN (the same afferent feedback signals are being used to control phase transition at the RG level of the ipsilateral CPG). These interneurons mediate inhibitory and excitatory actions to the flexor parts of the contralateral locomotor CPG at the RG and PFs levels, namely to the following interneurons: RG-F, Inrg-F; PF-hF, Inpf-hF; PF-kF, Inpf-kF; PF-aF, Inpf-aF; PF-BFP, In-eF, In-lF (see Fig. 2.7).

Previously, it has been suggested that cutaneous afferents are also involved in the coordination between left and right sides of locomotor circuitry by providing polysynaptic actions onto the flexor part of the contralateral CPG (Bouyer and Rossignol 2003a, b). Therefore, we hypothesized that feedback from cutaneous paw pad afferents also provides excitatory action onto the flexor part of the contralateral locomotor CPG at the RG and PFs levels via the appropriate commissural interneurons (In-eCIN).

2.6   Neuromechanical Simulations of Cat Level Walking

The neuromechanical hindlimb model and the CPG model were interconnected through feedforward (from motoneurons to muscles) and feedback (from muscles to neural circuits) signals. Weights of feedback signals were adjusted manually to obtain stable locomotion and to match the simulated motoneuronal activity with the muscle electromyographic (EMG) activity recorded during walking. The weights of the feedback signals were tuned using muscle EMG activity and locomotor mechanical characteristics recorded in five cats during overground and treadmill walking. The experimental procedures were approved by the Institutional Animal Care and Use Committees of Drexel University and Georgia Institute of Technology and described, along with the experimental results, in details elsewhere (Gregor et al. 2006; Ollivier-Lanvin et al. 2011; Prilutsky et al. 2011; Markin et al. 2012; Prilutsky et al. 2015). Briefly, the animals were trained for 3–4 weeks to walk on a Plexiglas enclosed walkway with 3 embedded 6-component force plates (16×11 cm^2, 360 Hz sampling rate, Bertec, USA) with self-selected speed or on a treadmill at constant speed between 0.3 and 0.6 m/s. Kinematics of the two hindlimbs were recorded using a 6-camera motion capture system Vicon (120 Hz, UK) and reflective markers attached to the joints. After locomotor training, EMG electrodes were implanted in 9 muscles under aseptic conditions and isoflurane anesthesia, and walking mechanics and EMG activity (sampling rates 120 and 3000 Hz) were recorded and analyzed.

2.6.1   Model Performance

After adjusting weights of afferent feedback signals, the neuromechanical model demonstrated stable locomotion with realistic walking mechanics and muscle activity. An increase in the supra-spinal drive to the CPG in the model (Fig. 2.12) increased the speed of locomotion, so that the walking cycle duration decreased due to the shortening of the stance phase with a relatively constant swing phase. The computed joint angles and ground reaction forces during walking with speeds of 0.4 and 0.55 m/s (see Fig. 2.12a and b, respectively) showed peak values and patterns similar to those recorded in walking cats (Gregor et al. 2006; Prilutsky et al. 2011).
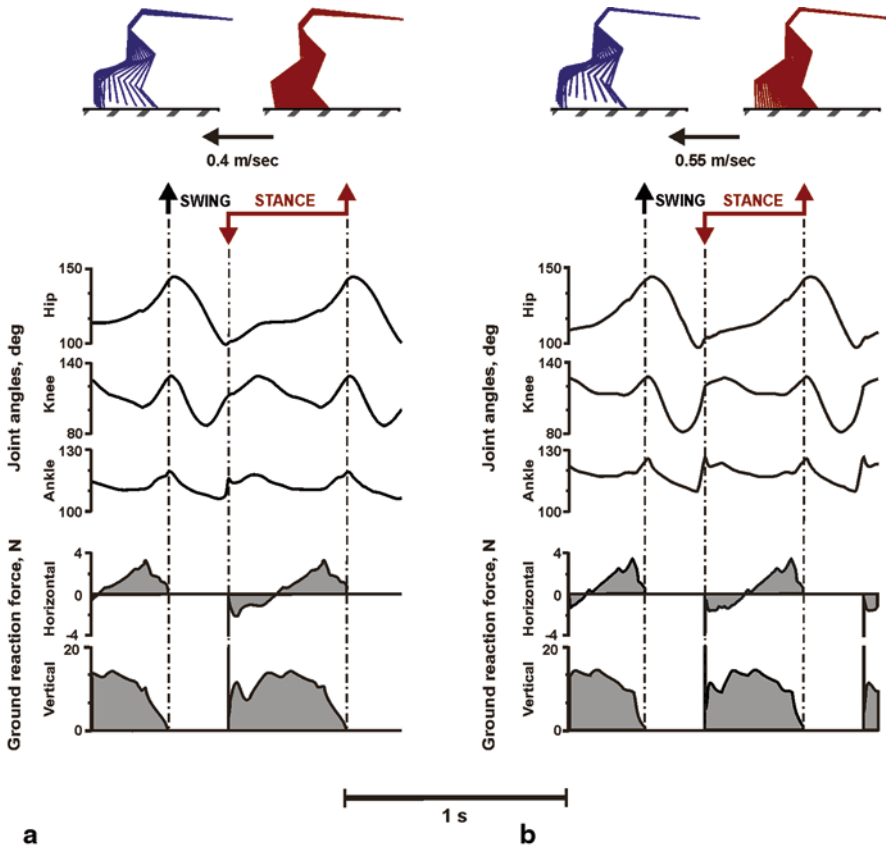
Fig. 2.12 Model performance at different speeds of treadmill locomotion: 0.4 m/s (**a**) and 0.55 m/s (**b**). The figure panels show (from *top* to *bottom*) stick figures, *joint angles*, and *horizontal* and *vertical* ground reaction forces. The simulated mechanics of walking closely match the experiment. (Gregor et al. 2006; Prilutsky et al. 2015)

Simulated patterns of muscle activity showed the correct phases of bursts and patterns similar to the recorded EMG (Markin et al. 2012) (Fig. 2.13).

2.6.2   Afferent Feedback Signals Controlling Phase Transitions

The neuromechanical model has been used for initial investigations of the effects of somatosensory afferent feedback on the control of locomotion. All results are obtained for a walking speed of 0.4 m/sec.

Our simulations have shown that the afferent feedback organization in the model and selected weights allow the model to maintain stable locomotion. Specifically, the transition between extensor and flexor phases in the CPG is mainly triggered

Fig. 2.13 Comparison of simulated (**a**) and recorded (**b**) patterns of normalized muscle activity obtained for walking on a treadmill (panel **b** reproduced with permission from (Markin et al. 2012)). Simulations were conducted for 0.4 m/s walking speed. All muscles of the model demonstrated the correct phases of activity and patterns similar to the recorded EMGs

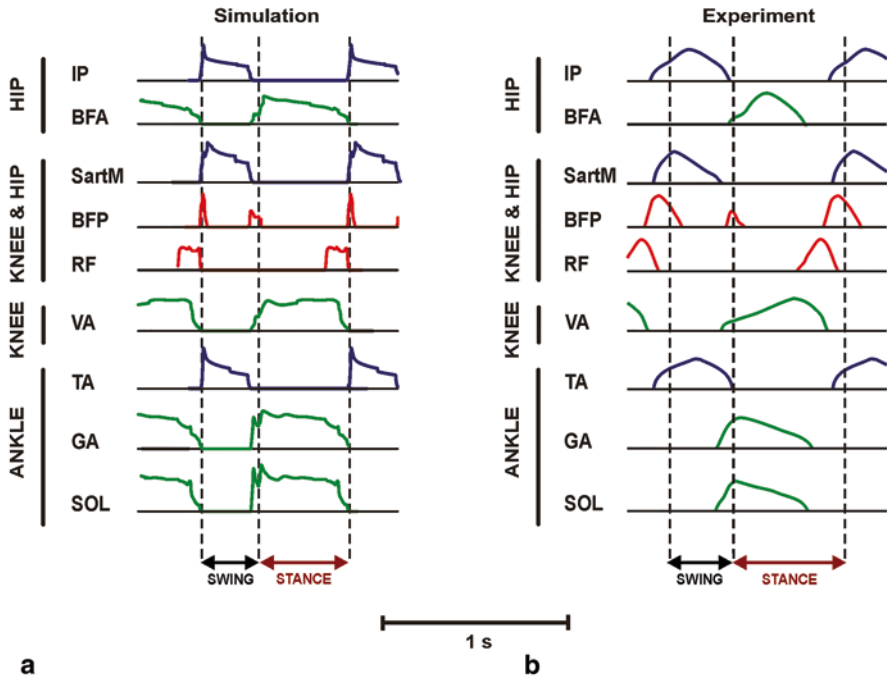by the length- and velocity-dependent afferent activity of IP (see Fig. 2.14). The force-dependent afferent feedback from ankle extensors (SOL and GA) and *cutaneous* paw pad feedback signal also contribute to the control of the transition between extensor and flexor phases by prolonging the duration of the extensor phase. In contrast, the timing of the flexor-extensor transition in the CPG is controlled by the length- and velocity-dependent hip extensor afferent activity (BFA) which adjusts the duration of flexor phase to limb kinematics during swing phase.

Further analysis of the possible role of afferent feedback signals in controlling phase transitions during normal locomotion has shown that some of them are critical for providing stable locomotion during level walking. In our computational experiments we selectively blocked the specific length- and load-sensitive afferent pathways at the RG level of CPG during locomotion by setting the corresponding synaptic weights to zero. The results of selective blocking the afferent feedback signals are presented in Fig. 2.15. The kinematics of the model is shown in the left panels of the figure by stick diagrams. The blue stick figures represent the model performance under normal conditions. After 40 s of steady-state locomotion, the specific afferent feedback signals are blocked at the RG levels of both left and right hindlimbs' CPGs. The behavior of the cat model after blocking the specific afferent signal is shown by red stick figures. The right panels of Fig. 2.15 represent the
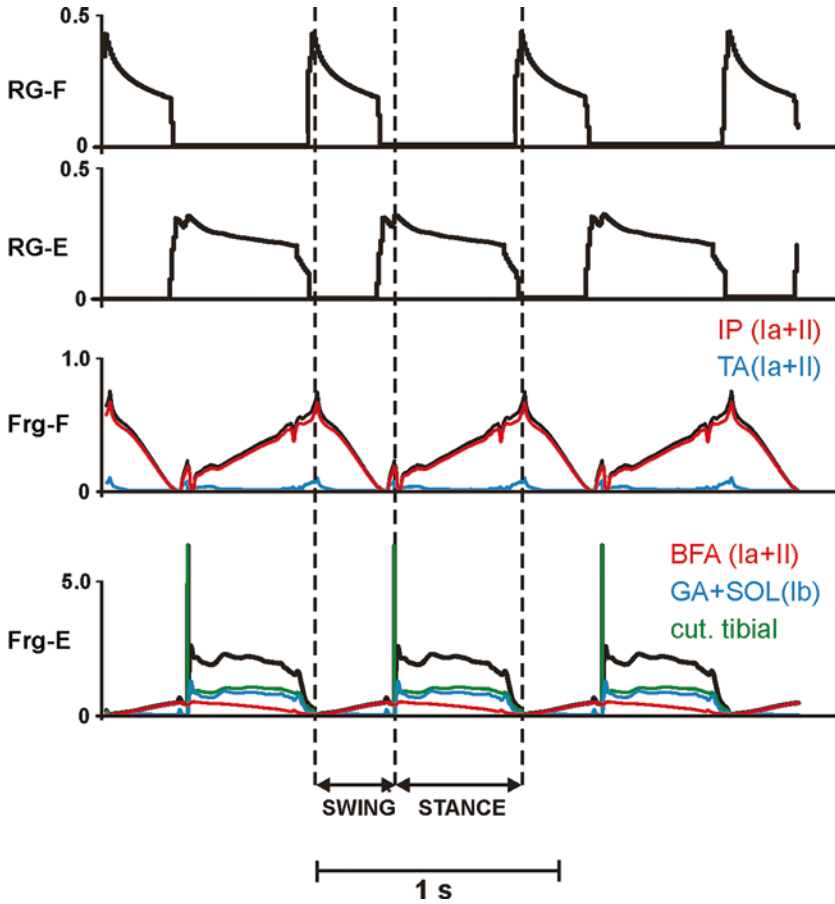
Fig. 2.14 Rhythmic activity of RG neurons (RG-F and RG-E) and normalized feedback signals to corresponding interneurons (Frg-F and Frg-E) during locomotion (see Fig. 2.5). The activity of RG-F and RG-E represent changes of the output neural variable of each neuron $f(V)$. The summarized afferent feedback inputs to both Frg-F and Frg-E interneurons are represented by *black lines*. The afferent feedback signals from different sources are shown by *red*, IP (Ia + II) or BFA (Ia + II); *blue*, TA (Ia + II) or GA + SOL (Ib); and *green* (cutaneous) *lines*. The *vertical dashed lines* separate the swing and stance phases

swing and stance phase durations of each cycle before and after blocking the corresponding afferent signals.

  After blocking feedback of group I and II afferents from both IP and TA muscles, the duration of stance phase increased at the afferent block onset (see right panel of Fig. 2.15a), whereas the duration of the swing phase in the first stride after the afferent block did not change. The model could produce only 2 strides without length-dependent feedback from IP and TA muscles.

  The removal of length-sensitive spindle afferents of the hip extensor (see Fig. 2.15b) affects the swing-stance phase transition. Namely, it increases the swing
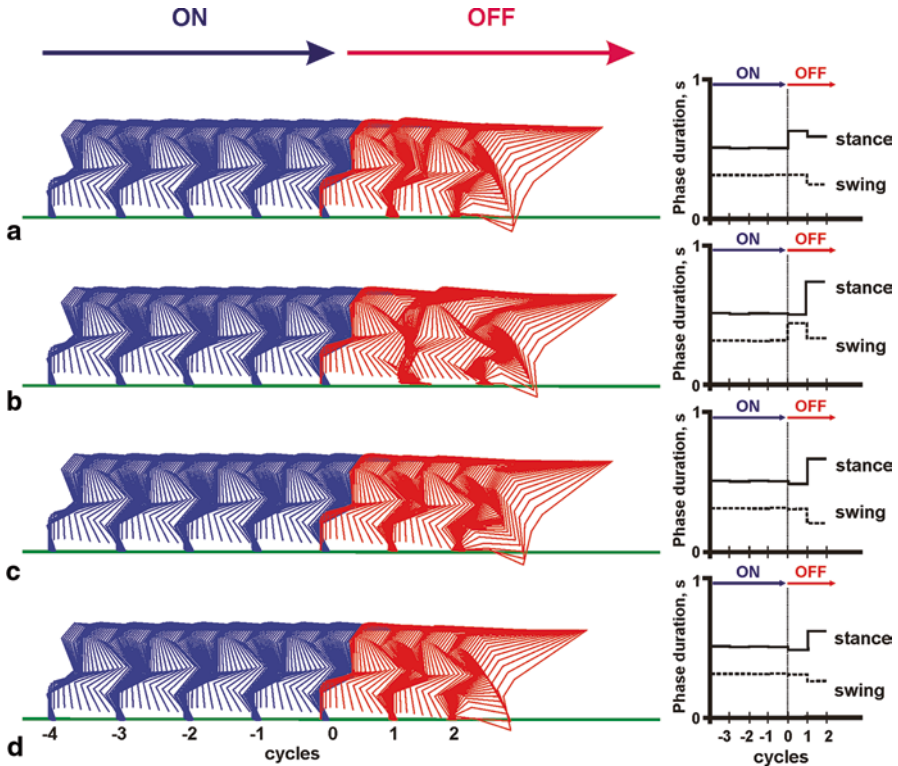
Fig. 2.15 The role of specific afferent feedback signals in maintaining stable locomotion. The *left* panel shows walking kinematics of the model before (*blue stick* figures) and after (*red stick* figures) blocking specific afferent feedback signals at the RG level. The *right* panel shows swing (*dotted lines*) and stance (*solid lines*) phase durations of each walking cycle before and after blocking the corresponding afferent signal. **a** Both IP and TA primary and secondary spindle afferents (Ia and II) are blocked; **b** BFA primary spindle afferents (Ia) are blocked; **c** Both SOL and GA Ib afferents are blocked; **d** Cutaneous paw pad afferents are blocked. Here and further cycle 0 indicates the onset of blocking the corresponding afferent signal(s)

duration after blocking the correspondent afferents and causes the cat model to collapse after 2 strides. The changes in stance and swing phase durations shown in Fig. 2.15a and b are in agreement with physiological experiments in which hip flexion and extension phases during locomotion were perturbed to modulate the afferent input from hip flexors and extensors (Perreault et al. 1995; Lam and Pearson 2002; McVea et al. 2005; Gregor et al. 2006). Our computer simulation experiments have also shown that the contribution of afferent feedback activity to regulation of the stance-swing transition is much greater from IP than from TA (Fig. 2.14), which contradicts the experimental data obtained in fictive locomotion preparations (Perreault et al. 1995; Stecina et al. 2005).

Figures 2.15c and d demonstrate model behavior after block of group Ib afferent pathways from ankle extensors (SOL/GA) and from *cutaneous paw pad* afferents,
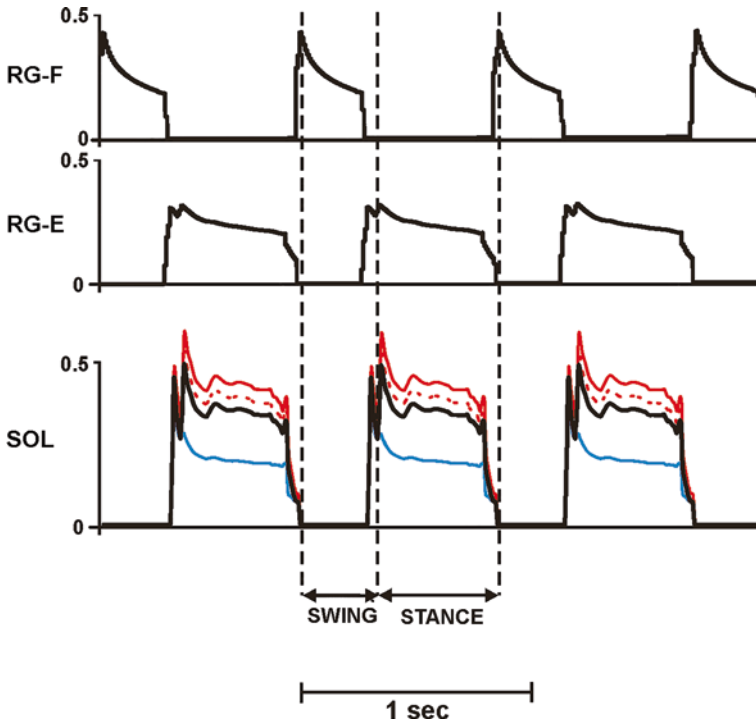
Fig. 2.16 Regulation of activity of soleus motoneuron (*SOL*) by disynaptic excitation and Renshaw cells. The *upper* and *middle* traces represent activity of the output neural variable *f*(V) of the principal neurons at RG level. The *lower* traces represent normalized activity of *SOL* motoneuron with and without the disynaptic excitation or recurrent inhibition from Renshaw cells: *black* and *blue lines* indicate *SOL* motoneuron activity with and without the effects of disynaptic excitation, respectively; *red* continuous and *dashed lines* show *SOL* motoneuron activity when all Renshaw cells are completely inhibited and when only Renshaw cells of agonistic motoneurons are blocked, respectively. The *vertical dashed lines* separate the *swing* and *stance* phases

correspondingly. Both feedback signals play similar roles in regulating the phase transition and are responsible for prolongation of the stance phase. The stance phase duration (see right panel of Fig. 2.15c and d) is slightly reduced in the first stride after blocking either Ib afferents from SOL and GA or *cutaneous paw pad* afferents, whereas the duration of the swing phase is relatively stable. The block of either feedback signal also causes the cat model to collapse after the second walking stride.

2.6.3 Regulation of Motoneuron Activity by Disynaptic Excitation and Renshaw Cells

Computer simulation experiments with the neuromechanical model have also shown the importance of afferent feedback for maintaining the ongoing motor activity during the stance phase of locomotion. Figure 2.16 demonstrates the activity
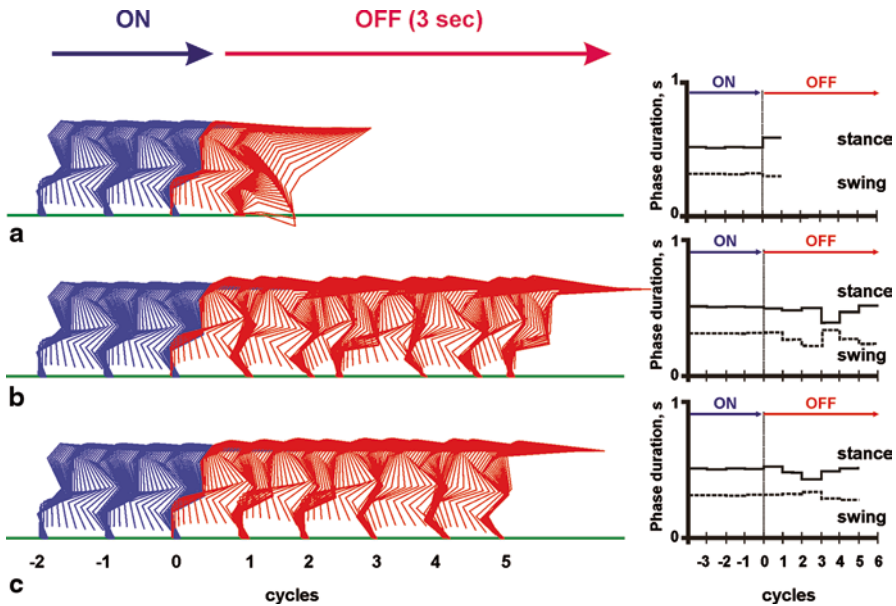
Fig. 2.17 Regulation of motoneuronal activity by the disynaptic excitation and recurrent inhibition during locomotion. The *left* panel represents simulated kinematics of the model before (*blue stick figures*) and after (*red stick figures*) blocking the disynaptic excitation or recurrent inhibition. The *right* panel represents *swing* (*dotted lines*) and *stance* (*solid lines*) phase durations of each simulated walking cycle before and after the blocking intervention. **a** Blocking the disynaptic excitatory feedback from group Ia and Ib afferents from all extensor muscles that normally reinforces motor activity during the extensor phase. **b** All Renshaw cells are completely inhibited. **c** Renshaw cells of agonist motoneurons are blocked

of SOL motoneuron with and without inputs from group Ib (or Ia and Ib) afferents from SOL muscle that provide disynaptic excitation of hindlimb extensor motoneurons during the stance phase. The obtained contribution of disynaptic excitation to the amplitude of SOL motoneuronal activity is about 30 %, which is similar to the afferent contributions estimated in other experimental and computational studies (Stein et al. 2000; Yakovenko et al. 2004).

Our simulations show that Renshaw cells may play an important role during locomotion. According to results of computational experiments (Fig. 2.16), Renshaw cells reduce the activity of synergistic motoneurons by recurrent inhibition, whereas inhibition of Renshaw cells by antagonistic motoneuron pools reduces Renshaw cell inhibitory influences on the synergist motoneurons.

Other reflex pathways included in the model—monosynaptic stretch reflex, non-reciprocal Ib-inhibition, have negligible contribution to regulation of the amplitude of motoneuronal activity.

In order to investigate how locomotor behavior of the model depends on the disynaptic excitation during the extensor phase and on Renshaw cell activity, we selectively switch off these pathways to all motoneurons for 3 s after 40 s of intact walking simulations (see Fig. 2.17). The results of selective blocking load-

dependent disynaptic excitation of extensor motoneurons demonstrate the importance of these feedback signals in providing weight support during the stance phase of locomotion. After blocking the extensor group I disynaptic pathway, the model was able to perform only one stride and then collapsed (Fig. 2.17a). Interestingly, the stance phase duration in these conditions increases, whereas the swing phase duration practically does not change (see Fig. 2.17a, right panel). In addition, the simulations have shown that *cutaneous* input from the paw pad also plays a crucial role in weight support during locomotion. Blocking the *cutaneous paw pad* pathway (see Fig. 2.8), which reinforces the ongoing extensor motor activity during stance phase, also results in collapse of the system. The model performance in this case is very similar to blocking the disynaptic excitation (see Fig. 2.17a).

Renshaw cells appear to be mostly responsible for regulating stability of locomotion. In our computational experiments, turning off the Renshaw cell pathways, which either inhibit the synergist motoneurons or inhibit the antagonist Renshaw cells (Fig. 2.9), affects the model walking kinematics (see Fig. 2.17b and c, left panels). In both cases, the flexor and extensor motoneurons are overexcited, which distorts walking kinematics. It is interesting to note that turning off all Renshaw cells (Fig. 2.17b) brings the system into a less stable locomotion regime compared to the situation when only the inhibitory pathways to the agonistic Renshaw cells are blocked (Fig. 2.17c). For example, the comparison of swing and stance phase durations in both cases shows that they become more variable than in the control condition (see Fig. 2.17b and c, right panels). Depending on the onset time of the Renshaw pathway block and its duration, the model may collapse after several walking cycles.

2.6.4 Role of Length-Dependent Ia and Force-Dependent Ib Triceps Surae Afferents in Controlling Locomotor Activity

The relative contribution of length-dependent (Ia) and force-dependent (Ib) muscle afferents in the control of locomotor activity is difficult to establish experimentally due to similar activation thresholds of these afferents and simultaneous increases in muscle length and force during muscle stretch. In order to illustrate how the role of Ia and Ib afferents of triceps surae muscle (SOL+GA) in controlling locomotion can be studied using the developed neuromechanical model, the following computational experiments were performed. After 40 s of steady-state locomotion, the pathways from triceps surae group I afferents were selectively blocked for 6 s. Specifically, we selectively blocked Ib feedback signals from GA and SOL muscles which projected onto the circuitry of (1) disynaptic excitation and (2) pattern formation network. Also, (3) all pathways of Ia feedback signals from triceps surae were blocked. Model performance is shown as stick figures in Fig. (2.18a) and the stance and swing phase
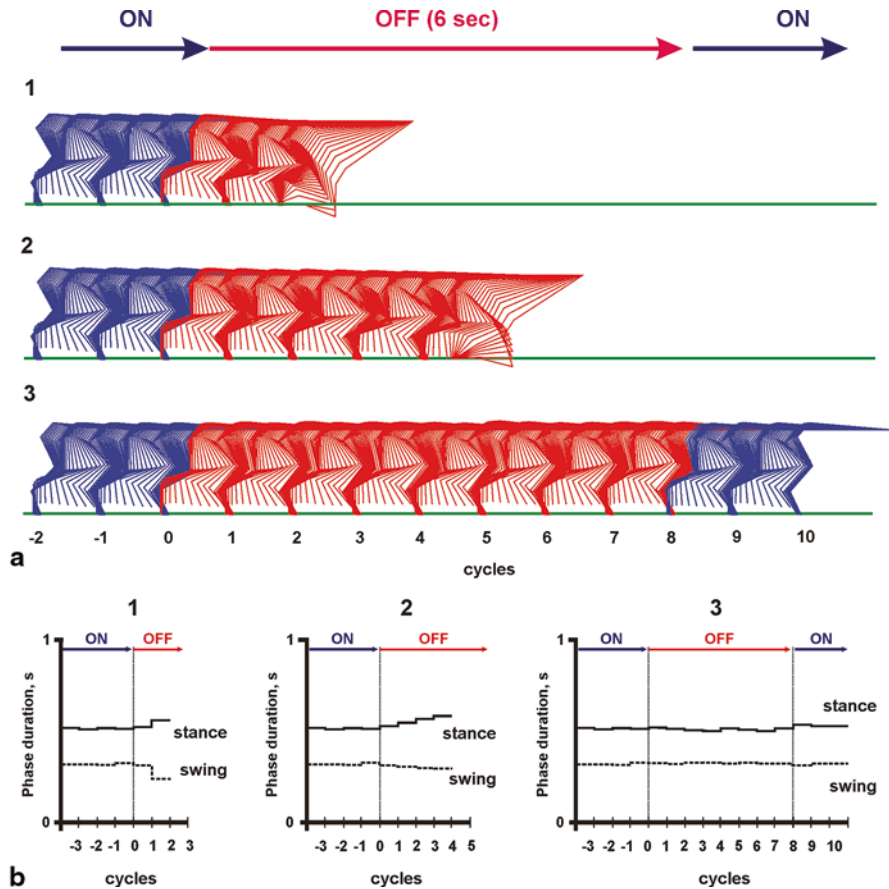
Fig. 2.18 Stick-figure diagrams (**a**) and cycle phase durations (**b**) of simulated walking before (*blue stick figures*) and after (*red stick figures*) selective removal of Ia and Ib feedback signals from the triceps surae muscle. *(1)* The disynaptic excitation circuitry does not receive triceps Ib afferent input; *(2)* the pattern formation circuitry does not receive triceps Ib afferent input; *(3)* all levels of the locomotor CPG do not receive triceps Ia afferent input

durations (Fig. 2.18b) for the above three cases of selective removal of afferent pathways.

Based on these computer experiments we concluded that selective removal of Ia feedback signals from triceps surae muscle should not substantially change the activity patterns of this and other muscles and the model maintains stable locomotion (Fig. 2.18a3 and b3). On the other hand, when the Ib afferent feedback signals from triceps surae were reduced to zero, the model was unable to produce stable locomotion and collapsed after several strides. Moreover, according to the model, different Ib pathways play different roles in providing stable locomotion. For example, Ib

feedback signals from GA and SOL muscles projecting onto the autogenic circuitry of disynaptic excitation were critical for reinforcement of ongoing GA-SOL motoneuronal activity (Fig. 2.18a1 and b1). The projection of Ib feedback signals from triceps surae onto the pattern formation network played an important role in regulation of the stance phase duration during level locomotion. The results of selective removal of this pathway (see Fig. 2.18b2) showed that the duration of stance phase was gradually increasing in each cycle after removal of this feedback eventually leading to collapse of the system after four walking cycles. Some of simulation results with selective removal of Ia afferent signals from SOL and GA (see Fig. 2.18) can be compared with experiments in which the monosynaptic action of Ia afferents is removed by self-reinnervation of these muscles in the cat (Abelew et al. 2000; Maas et al. 2007). In these studies, the muscle nerves were transected and surgically repaired and the proximal nerve stumps were allowed to regenerate for at least 3 months, an amount of time sufficient for reinnervation of the denervated muscle (Gordon and Stein 1982; O'Donovan et al. 1985). This self-reinnervation procedure removes the monosynaptic stretch reflex from self-reinnervated muscles (Cope and Clark 1993; Cope et al. 1994) due to permanent loss of Ia synapses on the cell bodies of motoneurons (Alvarez et al. 2011). Self-reinnervation of the entire triceps surae (Abelew et al. 2000), two heads of GA, medial gastrocnemius and lateral gastrocnemius, (Maas et al. 2007) or SOL and lateral gastrocnemius (Gregor et al. 2014) does not cause noticeable changes in hindlimb kinematics during level walking (Fig. 2.19), however an excessive ankle yield in stance during downslope walking has been reported (Abelew et al. 2000; Maas et al. 2007). Hindlimb joint angles during simulated walking with (blue lines) and without Ia input (red lines) from SOL and GA (Fig. 2.19a) have similar patterns and magnitudes and closely resemble joint angles recorded during walking of a representative cat before (blue lines) and after self-reinnervation of SOL and lateral gastrocnemius muscles (red lines, Fig. 2.19b).

2.7 Conclusion

This chapter describes a comprehensive neuromechanical model of spinal neural control of locomotion. The neuromechanical model includes a model of spinal circuits with the locomotor central pattern generator (Rybak et al. 2006a, b) controlled by afferent signals from 18 hindlimb Hill-type muscle actuators (Prilutsky et al. 2015). The spinal network incorporates basic circuits involved in the monosynaptic stretch reflex, Ia reciprocal inhibition, recurrent inhibition via Renshaw cells, and disynaptic excitation of extensor muscles via Ia and Ib afferents.

A special care was taken to tune model parameters since many of them cannot be determined experimentally. Three groups of model parameters, representing parameters of three subsystems of the model, were tuned independently. Parameters
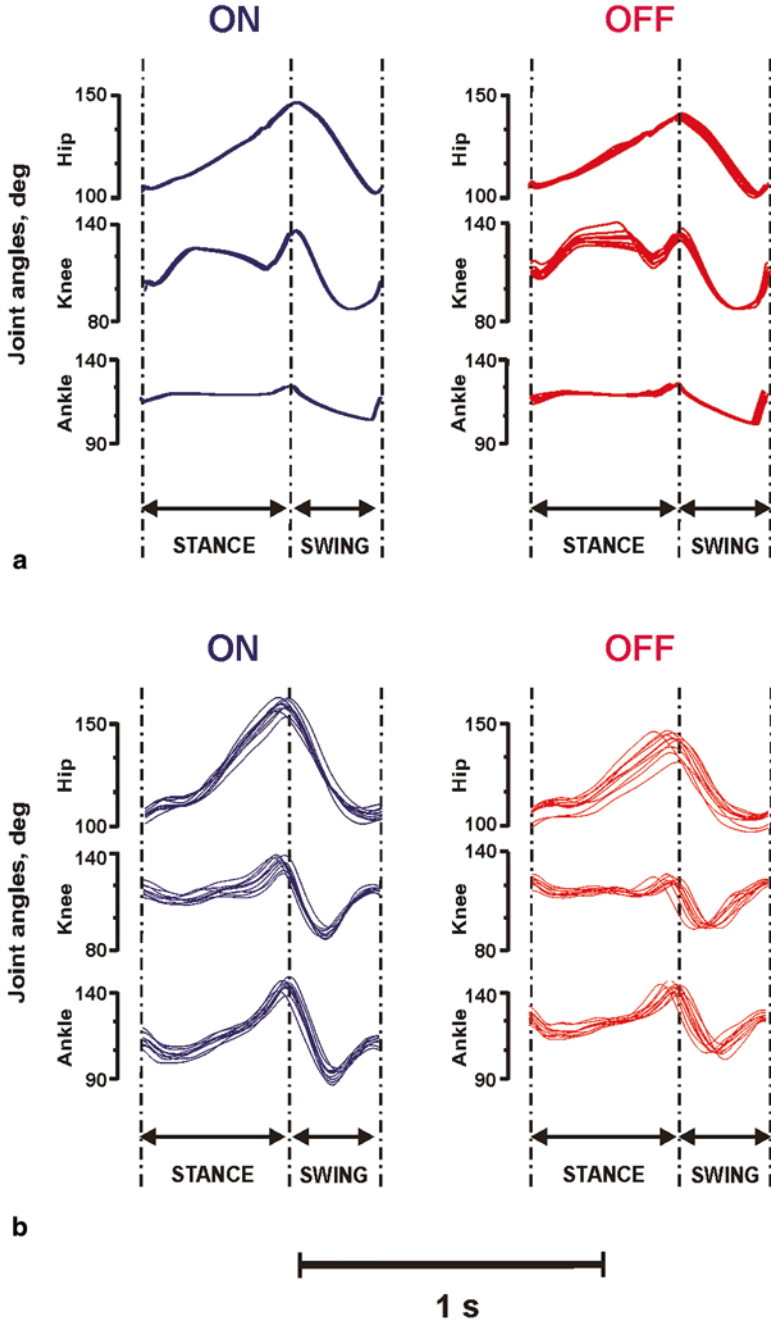
Fig. 2.19 Comparison of simulated (**a**) and recorded (**b**) hindlimb joint angles during a cycle of level walking before (*blue lines*) and after (*red lines*) removal of Ia afferent input from GA and SOL muscles. Simulated joint angles are shown for 10 consecutive cycles of walking at 0.4 m/s.

of the CPG model were manually selected to reproduce the effects of deletions and afferent stimulations observed during fictive locomotion in the cat (Rybak et al. 2006a, b). Parameters of the musculoskeletal model of the hindlimbs were optimized so that the difference between computed and recorded joint angles, muscle fascicle length changes, joint moments, and ground reaction forces during walking in the cat is minimized (Prilutsky et al. 2015). Finally, weight coefficients of motion-dependent sensory feedback signals to the spinal circuits were manually tuned without changing the parameters of the CPG and musculoskeletal models to reproduce realistic locomotor patterns of muscle activity and mechanical characteristics of locomotion.

The model provides important insights into the neural mechanisms for control of locomotion and can be used as a testbed to study control of locomotion in normal and pathological conditions.

In experiments, Ia afferent input was removed by self-reinnervation of SOL and lateral gastrocnemius muscles in the cat (Cope et al. 1994; Maas et al. 2007; Alvarez et al. 2011). The experimental data are unpublished results from Prilutsky's laboratory. The experimental procedures have been described in details elsewhere (Maas et al. 2007; Prilutsky et al. 2011). Experimental joint angles are shown for 10 cycles of level walking with self-selected speed recorded before (mean±SD speed: 0.571 ± 0.082 m/s) and at least 12 weeks after self-reinnervation of SOL and lateral gastrocnemius muscles (0.573 ± 0.026 m/s)

APPENDIX 2 Parameters of Locomotor Circuitry

Neuronal parameters of locomotor circuitry are based on parameters of simplified version of the CPG model described in (Markin et al. 2010).

Table 2.1 Weights of synaptic connections within rhythm generator circuitry. (see Figs. 2.5 and 2.6)

Targets	RG-F	RG-E	Inrg-F	Inrg-E
Sources	*Excitatory*			
Drive	0.12	0.12		
RG-F	0.01		0.4	
RG-E		0.01		0.4
Frg-F	0.16		0.12	
Frg-E		0.44		0.28
	Inhibitory			
Inrg-F		2.1		
Inrg-E	2.1			

Table 2.2 Weights of synaptic connections within pattern formation circuitry that controls hip synergists. (see Figs. 2.5 and 2.7)

Targets	PFh-F	PFh-E	Inpf-hF	Inpf-hE
Sources	*Excitatory*			
Drive	0.62	0.62		
RG-F	0.5			
RG-E		0.5		
PF-hF			0.4	
PF-hE				0.4
Fpf-hF	0.05		0.15	
Fpf-hE		0.17		0.25
Fpf-cut		0.19		
	Inhibitory			
Inrg-F		1.2		
Inrg -E	1.2			
Inpf-hF		4.5		
Inpf-hE	4.5			

Table 2.3 Weights of synaptic connections within pattern formation circuitry that controls knee synergists. (see Figs. 2.5 and 2.7)

Targets	PFk-F	PFk-E	Inpf-kF	Inpf-kE
Sources	*Excitatory*			
Drive	0.62	0.62		
RG-F	0.3			
RG-E		0.3		
PF-kF			0.4	
PF-kE				0.4
Fpf-kF	0.12		0.25	
Fpf-kE		0.55		0.47
Fpf-cut				0.22
	Inhibitory			
Inrg-F		1.6		
Inrg-E	1.6			
Inpf-kF		3.4		
Inpf-kE	3.4			

Table 2.4 Weights of synaptic connections within pattern formation circuitry that controls ankle synergists. (see Figs. 2.5 and 2.7)

Targets	PF-aF	PF-aE	Inpf-aF	Inpf-aE
Sources	*Excitatory*			
Drive	0.6	0.6		
RG-F	0.4			
RG-E		0.4		
PF-aF			0.4	
PF-aE				0.4
Fpf-aF	0.2		1.0	
Fpf-aE		0.45		0.25
Fpf-cut				0.1
	Inhibitory			
Inrg-F		2.6		
Inrg-E	2.6			
Inpf-aF		3.9		
Inpf-aE	3.9			

Table 2.5 Weights of synaptic connections within pattern formation circuitry that specifically controls two-joint BFP and RF muscles. (see Figs. 2.5 and 2.7)

Targets	PF-BFP	PF-RF	In-eF	In-lF	In-eE	In-lE
Sources	*Excitatory*					
Drive	0.04	0.09				
RG-F	0.5	0.06	0.14	0.08		
RG-E	0.5	0.9			0.4	
PF-BFP						
PF-RF						
Fpf-rf		0.3			0.2	
Fpf-bfp	0.2		0.2			0.1
	Inhibitory					
Inrg-F		1.3			0.3	3.3
Inrg-E	1.2		1.4	3.5		1.2
In-eF				1.0		
In-lF	3.9	1.8	2.7			
In-eE		3.1				0.8
In-lE	0.4				3.6	

Table 2.6 Weights of synaptic connections within disynaptic excitation and weight support circuitry (excluding motoneurons). (see Fig. 2.8)

Targets	PFh-E	PFk-E	PFa-E	Iab-BFA	Iab-VA	Iab-GA	Iab-SOL	In-de
Sources	*Excitatory*							
Drive								0.2
RG-E								
PFh-E				0.26				
PFk-E					0.26			
PFa-E						0.26	0.24	
Fpf-cut	0.19	0.22	0.12					
	Inhibitory							
Inrg-E								0.3
In-de				0.8	0.8	0.8	0.8	

Table 2.7 Weights of synaptic connections within reflexes circuitry (including motoneurons). (see Figs. 2.9 and 2.10)

Targets	Mn-IP	RC-IP	Ia-IP	Ib-IP-
Sources	*Excitatory*			
PF-hF	1.6		0.3	0.35
Mn-IP		0.2		
Ib-BFP +	0.1			
	Inhibitory			
Inpf-hF		0.03		
RC-IP	0.3		0.2	
RC-SartM	0.15			
RC-TA	0.23			
RC-BFA		0.1		
Ia-BFA	0.2		0.2	
Ib-IP-	0.3			
Ib-RF-	0.9			
	IP afferents			
Ia	0.2		0.4	
Ib				0.4

Targets	Mn-SartM	RC-SartM	Ia-SartM	Ib-SartM-
Sources	*Excitatory*			
PF-hF	0.9		0.1	0.1
PF-kF	1.0		0.2	0.27
Mn-SartM		0.2		
	Inhibitory			
Inpf-hF		0.01		
Inpf-kF		0.02		
RC-SartM	0.2		0.2	
RC-IP	0.15			
RC-TA	0.1			
RC-VA		0.2		
RC-BFA		0.1		
Ia-VA	0.2		0.15	
Ia-RF	0.2		0.1	
Ia-BFA	0.1		0.1	
Ib-SartM-	0.17			
Ib-BFP-	0.8			
	SartM afferents			
Ia	0.1		0.1	
Ib				0.23

Targets	Mn-BFA	RC-BFA	Ia-BFA
Sources	*Excitatory*		
PF-hE	1.8		0.4
Mn-BFA		0.2	
Iab-BFA	0.5		
	Inhibitory		
Inpf-hE		0.04	
RC-IP		0.1	
RC-BFA	0.2		0.2
RC-VA	0.08		
RC-GA	0.09		
RC-SOL	0.14		
Ia-IP	0.25		0.2
Ia-SartM	0.15		0.15
Ib-BFP-	1.1		
	BFA afferents		
Ia	0.2		0.2

Targets	Mn-BFP	RC-BFP	Ia-BFP	Ib-BFP-	Ib-BFP+
Sources	*Excitatory*				
PF-BFP	1.4		0.8	0.1	0.1
Mn-BFP		0.2			
	Inhibitory				
RC-BFP	0.2		0.2		
RC-RF		0.2			
Ia-RF	0.2		0.2		
Ia-SartM	0.15		0.05		
	BFP afferents				
Ia	0.13		0.1		
Ib				0.7	0.7

Targets	Mn-RF	RC-RF	Ia-RF	Ib-RF-
Sources	*Excitatory*			
PF-RF	1.6		0.85	0.1
Mn-RF		0.2		
	Inhibitory			
RC-RF	0.2		0.2	
RC-BFP		0.2		
Ia-GA	0.1		0.1	
Ia-BFP	0.2		0.2	
	RF afferents			
Ia	0.15		0.3	
Ib				0.6

Targets	Mn-VA	RC-VA	Ia-VA	Ib-VA-
Sources	*Excitatory*			
PF-kE	1.75		0.37	0.1
Mn-VA		0.2		
Iab-VA	0.43			
Ib-GA +	0.09			
	Inhibitory			
Inpf-kE				
RC-SartM	0.2	0.2		
RC-VA	0.2		0.2	
RC-BFA	0.09			
RC-GA	0.14			
RC-SOL	0.06			
Ia-GA	0.1		0.1	
Ia-BFP	0.3			
Ia-SartM	0.22		0.02	
Ib-RF-	0.1			
	VA afferents			
Ia	0.13		0.1	
Ib				0.1

Targets	Mn-GA	RC-GA	Ia-GA	Ib-GA-	Ib-GA +
Sources	*Excit-atory*				
PF-kF	0.2		0.05	0.01	0.01
PF-aE	1.5		0.45	0.1	0.1
Mn-GA		0.2			
Iab-GA	0.33				
	Inhibitory				
Inpf-aE		0.06			
Inpf-kF		0.01			
RC-TA	0.1	0.1			
RC-GA	0.2		0.2		
RC-BFA	0.1				
RC-VA	0.06				
RC-SOL	0.06				
Ia-TA	0.3		0.2		
Ia-RF	0.2		0.2		
Ia-VA	0.1		0.2		
	GA afferents				
Ia	0.2		0.2		
Ib				0.25	0.15

Targets	Mn-TA	RC-TA	Ia-TA	Ib-TA-
Sources	*Excitatory*			
PF-aF	2.1		0.6	0.4
Mn-TA		0.2		
Ib-GA +	0.1			
	Inhibitory			
Inpf-aF		0.03		
RC-TA	0.3		0.2	
RC-IP	0.2			
RC-SartM	0.1			
Ia-GA	0.2	0.1	0.2	
Ia-SOL	0.5	0.1	0.2	
Ib-TA-	0.2			
	TA afferents			
Ia	0.1		0.3	
Ib				0.35

Targets	Mn-SOL	RC-SOL	Ia-SOL	Ib-SOL-
Sources	*Excitatory*			
PF-aE	1.75		0.37	0.1
Mn-SOL		0.2		
Iab-SOL	0.31			
	Inhibitory			
Inpf-aE		0.05		
RC-TA		0.1		
RC-SOL	0.2		0.2	
RC-BFA	0.1			
RC-VA	0.04			
RC-GA	0.08			
Ia-TA	0.5		0.2	
Ib-GA-	0.23			
	SOL afferents			
Ia	0.21		0.3	
Ib				0.1

Table 2.8 Weights of synaptic connections within left-right coordination circuitry. (see Fig. 2.11)

Trg	(c)RG-F	(c)Inrg-F	(c)PF-hF	(c)Inpf-hF	(c)PF-kF	(c) Inpf-kF	(c)PF-aF	(c) Inpf-aF
Src	*Excit-atory*							
In-eCIN	0.3	0.02	0.2	0.04	0.15	0.03	0.15	0.03
	Inhibitory							
In-iCIN	2.6	0.05	3.2	0.07	2.4	0.04	2.6	0.05

Table 2.9 Weights of synaptic connections feedbacks. (see Figs. 2.6, 2.7, 2.8, 2.10, and 2.11)

Targets	Frg-F	Frg-E	Fpf-hF	Fpf-hE	Fpf-kF
Sources	IP afferents				
Ia	0.43		0.15		
II	0.2		0.3		
	SartM afferents				
Ia					0.28
II					0.75
	BFA afferents				
Ia		0.06		0.06	
II		0.08		0.11	
Ib				0.1	
	GA afferents				
Ia					0.03
II					0.1
Ib		0.05			
	TA afferents				
Ia	0.1				
II	0.1				
	SOL afferents				
Ia					
Ib		0.18			
	Cutaneous				
		0.25			

	Fpf-kE	Fpf-aF	Fpf-aE	Fpf-bfp	Fpf-rf
	BFP afferents				
Ia				0.25	
II				0.15	
	RF afferents				
Ia					0.5
II					0.5
	VA afferents				
Ia	0.15				
II	0.24				
Ib	0.3				
	GA afferents				
Ia				0.02	
II				0.04	
Ib				0.05	
	TA afferents				
Ia		0.3			
II		0.6			
	SOL afferents				
Ia			0.03		
II			0.06		
Ib			0.07		

	Fpf-cut	Iab-BFA	Iab-VA	Iab-GA	Iab-SOL
BFA afferents					
Ia		0.02			
Ib		0.01			
VA afferents					
Ia			0.05		
Ib			0.31		
GA afferents					
Ia				0.28	
Ib				1.4	
TA afferents					
Ia					0.75
Ib					0.75
Cutaneous					
	1				

	In-eCIN	In-iCIN
IP afferents		
Ia		0.43
II		0.2
BFA afferents		
Ia	0.06	
II	0.08	
GA afferents		
Ib	0.05	
TA afferents		
Ia		0.1
II		0.1
SOL afferents		
Ib	0.18	
Cutaneous		
	0.25	

References

Abelew TA, Miller MD, Cope TC, Nichols TR (2000) Local loss of proprioception results in disruption of interjoint coordination during locomotion in the cat. J Neurophysiol 84:2709–2714

Alvarez FJ, Fyffe RE (2007) The continuing case for the Renshaw cell. J Physiol 584:31–45

Alvarez FJ, Titus-Mitchell HE, Bullinger KL, Kraszpulski M, Nardelli P, Cope TC (2011) Permanent central synaptic disconnection of proprioceptors after nerve injury and regeneration. I. Loss of VGLUT1/IA synapses on motoneurons. J Neurophysiol 106:2450–2470

Andersson O, Grillner S (1983) Peripheral control of the cat's step cycle. II. Entrainment of the central pattern generators for locomotion by sinusoidal hip movements during "fictive locomotion.". Acta Physiol Scand 118:229–239

Angel MJ, Guertin P, Jimenez I, McCrea DA (1996) Group I extensor afferents evoke disynaptic EPSPs in cat hindlimb extensor motorneurones during fictive locomotion. J Physiol 494(Pt 3):851–861

Aoi S (2015) Neuromusculoskeletal modeling for the adaptive control of posture during locomotion. In: Prilutsky BI, Edwards DH Jr (eds) Neuromechanical modeling of posture and locomotion. Springer, New York

Aoi S, Kondo T, Hayashi N, Yanagihara D, Aoki S, Yamaura H et al (2013) Contributions of phase resetting and interlimb coordination to the adaptive control of hindlimb obstacle avoidance during locomotion in rats: a simulation study. Biol Cybern 107:201–216

Baldissera F, Hultborn H, Illert M (1981) Integration in spinal neuronal systems. In: Brooks VB (ed) Handbook of physiology. Section 1: the nervous system. Vol. III. motor control, part 1. American Physiological Society, Washington, DC, pp 509–595

Baratta RV, Solomonow M, Best R, D'Ambrosia R (1993) Isotonic length/force models of nine different skeletal muscles. Med Biol Eng Comput 31:449–458

Baratta RV, Solomonow M, Best R, Zembo M, D'Ambrosia R (1995) Architecture-based force-velocity models of load-moving skeletal muscles. Clin Biomech (Bristol Avon) 10:149–155

Beer RD, Chiel HJ, Gallagher JC (1999) Evolution and analysis of model CPGs for walking: II. General principles and individual variability. J Comput Neurosci 7:119–147

Bouyer LJ, Rossignol S (2003a) Contribution of cutaneous inputs from the hindpaw to the control of locomotion. I. Intact cats. J Neurophysiol 90:3625–3639

Bouyer LJ, Rossignol S (2003b) Contribution of cutaneous inputs from the hindpaw to the control of locomotion. II. Spinal cats. J Neurophysiol 90:3640–3653

Brown TG (1911) The intrinsic factors in the act of progression in the mammal. Proc R Soc B 84:308–319

Brown IE, Liinamaa TL, Loeb GE (1996) Relationships between range of motion, lo, and passive force in five strap-like muscles of the feline hind limb. J Morphol 230:69–77

Burke RE (1999) The use of state-dependent modulation of spinal reflexes as a tool to investigate the organization of spinal interneurons. Exp Brain Res 128:263–277

Burke RE, Degtyarenko AM, Simon ES (2001) Patterns of locomotor drive to motoneurons and last-order interneurons: clues to the structure of the CPG. J Neurophysiol 86:447–462

Butt SJ, Kiehn O (2003) Functional identification of interneurons responsible for left-right coordination of hindlimbs in mammals. Neuron 38:953–963

Cohen AH, Holmes PJ, Rand RH (1982) The nature of the coupling between segmental oscillators of the lamprey spinal generator for locomotion: a mathematical model. J Math Biol 13:345–369

Collins JJ, Richmond SA (1994) Hard-wired central pattern generators for quadrupedal locomotion. Biol Cybern 71:375–385

Conway BA, Hultborn H, Kiehn O (1987) Proprioceptive input resets central locomotor rhythm in the spinal cat. Exp Brain Res 68:643–656

Cope TC, Clark BD (1993) Motor-unit recruitment in self-reinnervated muscle. J Neurophysiol 70:1787–1796

Cope TC, Bonasera SJ, Nichols TR (1994) Reinnervated muscles fail to produce stretch reflexes. J Neurophysiol 71:817–820

Corana A, Marchesi M, Martini C, Ridella S (1987) Minimizing multimodal functions of continu-
ous variables with the "simulated annealing" algorithm. ACM Trans Math Softw 13:263–280

Degtyarenko AM, Simon ES, Norden-Krichmar T, Burke RE (1998) Modulation of oligosynaptic
cutaneous and muscle afferent reflex pathways during fictive locomotion and scratching in the
cat. J Neurophysiol 79:447–463

Duysens J, Pearson KG (1980) Inhibition of flexor burst generation by loading ankle extensor
muscles in walking cats. Brain Res 187:321–332

Eccles RM, Lundberg A (1958) Integrative pattern of Ia synaptic actions on motoneurones of hip
and knee muscles. J Physiol 144:271–298

Eccles JC, Fatt P, Landgren S (1956) Central pathway for direct inhibitory action of impulses in
largest afferent nerve fibres to muscle. J Neurophysiol 19:75–98

Eccles JC, Eccles RM, Lundberg A (1957a) The convergence of monosynaptic excitatory afferents
on to many different species of alpha motoneurones. J Physiol 137:22–50

Eccles JC, Eccles RM, Lundberg A (1957b) Synaptic actions on motoneurones caused by impulses
in Golgi tendon organ afferents. J Physiol 138:227–252

Ekeberg O, Pearson K (2005) Computer simulation of stepping in the hind legs of the cat: an exam-
ination of mechanisms regulating the stance-to-swing transition. J Neurophysiol 94:4256–4268

Feldman AG, Orlovsky GN (1975) Activity of interneurons mediating reciprocal 1a inhibition dur-
ing locomotion. Brain Res 84:181–194

Fouad K, Pearson KG (1997) Effects of extensor muscle afferents on the timing of locomotor
activity during walking in adult rats. Brain Res 749:320–328

Frigon A, Sirois J, Gossard JP (2010) Effects of ankle and hip muscle afferent inputs on rhythm
generation during fictive locomotion. J Neurophysiol 103:1591–1605

Gordon T, Stein RB (1982) Time course and extent of recovery in reinnervated motor units of cat
triceps surae muscles. J Physiol 323:307–323

Gosgnach S, Quevedo J, Fedirchuk B, McCrea DA (2000) Depression of group Ia monosynaptic
EPSPs in cat hindlimb motoneurones during fictive locomotion. J Physiol 526(Pt 3):639–652

Gossard JP, Brownstone RM, Barajon I, Hultborn H (1994) Transmission in a locomotor-related
group Ib pathway from hindlimb extensor muscles in the cat. Exp Brain Res 98:213–228

Gossard JP, Sirois J, Noue P, Cote MP, Menard A, Leblond H et al (2011) Chapter 2-the spinal
generation of phases and cycle duration. Prog Brain Res 188:15–29

Gottschall JS, Nichols TR (2011) Neuromuscular strategies for the transitions between level and
hill surfaces during walking. Philos Trans R Soc Lond B Biol Sci 366:1565–1579

Gregor RJ, Smith DW, Prilutsky BI (2006) Mechanics of slope walking in the cat: quantification of
muscle load, length change, and ankle extensor EMG patterns. J Neurophysiol 95:1397–1409

Gregor RJ, Bulgakova MA, Maas H, Oliver A, Prilutsky BI (2014) Locomotor activity of feline
ankle extensors during level and slope walking after removal of stretch reflex
from soleus and lateral gastrocnemius by self-reinnervation. In: 2014 Neuroscience Meeting
Planner, Program # 827-01. (ed), Society for Neuroscience. Online, Washington, DC

Grillner S (1981) Control of locomotion in bipeds, tetrapods, and fish. In: Brooks V (ed) Hand-
book of physiology. Section I. The nervous system. American Physiological Society, Bethesda,
pp 1179–1236

Grillner S, Wallen P, Saitoh K, Kozlov A, Robertson B (2008) Neural bases of goal-directed loco-
motion in vertebrates-an overview. Brain Res Rev 57:2–12

Guertin PA (2012) Central pattern generator for locomotion: anatomical, physiological, and patho-
physiological considerations. Front Neurol 3:183

Guertin P, Angel MJ, Perreault MC, McCrea DA (1995) Ankle extensor group I afferents excite ex-
tensors throughout the hindlimb during fictive locomotion in the cat. J Physiol 487(Pt 1):197–
209

Hiebert GW, Pearson KG (1999) Contribution of sensory feedback to the generation of extensor
activity during walking in the decerebrate cat. J Neurophysiol 81:758–770

Hiebert GW, Whelan PJ, Prochazka A, Pearson KG (1996) Contribution of hind limb flexor muscle
afferents to the timing of phase transitions in the cat step cycle. J Neurophysiol 75:1126–1137

Hoy MG, Zernicke RF (1985) Modulation of limb dynamics in the swing phase of locomotion. J Biomech 18:49–60

Ivashko DG, Prilutsky BI, Markin SN, Chapin JK, Rybak IA (2003) Modeling the spinal cord neural circuitry controlling cat hindlimb movement during locomotion. Neurocomputing 52–54:621–629

Jami L (1992) Golgi tendon organs in mammalian skeletal muscle: functional properties and central actions. Physiol Rev 72:623–666

Jankowska E (1992) Interneuronal relay in spinal pathways from proprioceptors. Prog Neurobiol 38:335–378

Jankowska E, Bannatyne BA, Stecina K, Hammar I, Cabaj A, Maxwell DJ (2009) Commissural interneurons with input from group I and II muscle afferents in feline lumbar segments: neurotransmitters, projections and target cells. J Physiol 587:401–418

Kiehn O (2011) Development and functional organization of spinal locomotor circuits. Curr Opin Neurobiol 21:100–109

Kriellaars DJ, Brownstone RM, Noga BR, Jordan LM (1994) Mechanical entrainment of fictive locomotion in the decerebrate cat. J Neurophysiol 71:2074–2086

Lam T, Pearson KG (2002) Sartorius muscle afferents influence the amplitude and timing of flexor activity in walking decerebrate cats. Exp Brain Res 147:175–185

Lanuza GM, Gosgnach S, Pierani A, Jessell TM, Goulding M (2004) Genetic identification of spinal interneurons that coordinate left-right locomotor activity necessary for walking movements. Neuron 42:375–386

Lloyd DP (1946) Integrative pattern of excitation and inhibition in two-neuron reflex arcs. J Neurophysiol 9:439–444

Maas H, Prilutsky BI, Nichols TR, Gregor RJ (2007) The effects of self-reinnervation of cat medial and lateral gastrocnemius muscles on hindlimb kinematics in slope walking. Exp Brain Res 181:377–393

Markin SN, Klishko AN, Shevtsova NA, Lemay MA, Prilutsky BI, Rybak IA (2010) Afferent control of locomotor CPG: insights from a simple neuromechanical model. Ann N Y Acad Sci 1198:21–34

Markin SN, Lemay MA, Prilutsky BI, Rybak IA (2012) Motoneuronal and muscle synergies involved in cat hindlimb control during fictive and real locomotion: a comparison study. J Neurophysiol 107:2057–2071

Maufroy C, Kimura H, Takase K (2008) Towards a general neural controller for quadrupedal locomotion. Neural Netw 21:667–681

McCrea DA (2001) Spinal circuitry of sensorimotor control of locomotion. J Physiol 533:41–50

McCrea DA, Rybak IA (2007) Modeling the mammalian locomotor CPG: insights from mistakes and perturbations. Prog Brain Res 165:235–253

McCrea DA, Rybak IA (2008) Organization of mammalian locomotor rhythm and pattern generation. Brain Res Rev 57:134–146

McCrea DA, Pratt CA, Jordan LM (1980) Renshaw cell activity and recurrent effects on motoneurons during fictive locomotion. J Neurophysiol 44:475–488

McCrea DA, Shefchyk SJ, Stephens MJ, Pearson KG (1995) Disynaptic group I excitation of synergist ankle extensor motoneurones during fictive locomotion in the cat. J Physiol 487(Pt 2):527–539

McVea DA, Donelan JM, Tachibana A, Pearson KG (2005) A role for hip position in initiating the swing-to-stance transition in walking cats. J Neurophysiol 94:3497–3508

Menard A, Leblond H, Gossard JP (1999) The modulation of presynaptic inhibition in single muscle primary afferents during fictive locomotion in the cat. J Neurosci 19:391–400

Nassour J, Henaff P, Benouezdou F, Cheng G (2014) Multi-layered multi-pattern CPG for adaptive locomotion of humanoid robots. Biol Cybern 108(3):291–303

Nichols TR, Bunderson N, Lyle M (2015) Neural regulation of limb mechanics: insights from the organization of proprioceptive circuits. In: Prilutsky BI, Edwards DH Jr (eds) Neuromechanical modeling of posture and locomotion. Springer, New York

Nichols TR, Cope TC, Abelew TA (1999) Rapid spinal mechanisms of motor coordination. Exerc Sport Sci Rev 27:255–284

Nishimaru H, Restrepo CE, Kiehn O (2006) Activity of Renshaw cells during locomotor-like rhythmic activity in the isolated spinal cord of neonatal mice. J Neurosci 26:5320–5328

O'Donovan MJ, Pinter MJ, Dum RP, Burke RE (1985) Kinesiological studies of self- and cross-reinnervated FDL and soleus muscles in freely moving cats. J Neurophysiol 54:852–866

Ollivier-Lanvin K, Krupka AJ, AuYong N, Miller K, Prilutsky BI, Lemay MA (2011) Electrical stimulation of the sural cutaneous afferent nerve controls the amplitude and onset of the swing phase of locomotion in the spinal cat. J Neurophysiol 105:2297–2308

Orlovsky GN, Deliagina TG, Grillner S (1999) Neuronal control of locomotion: from mollusc to man. Oxford University Press, New York

Pearson KG (1995) Proprioceptive regulation of locomotion. Curr Opin Neurobiol 5:786–791

Pearson KG (2008) Role of sensory feedback in the control of stance duration in walking cats. Brain Res Rev 57:222–227

Pearson KG, Collins DF (1993) Reversal of the influence of group Ib afferents from plantaris on activity in medial gastrocnemius muscle during locomotor activity. J Neurophysiol 70:1009–1017

Pearson KG, Misiaszek JE, Fouad K (1998) Enhancement and resetting of locomotor activity by muscle afferents. Ann N Y Acad Sci 860:203–215

Perreault MC, Angel MJ, Guertin P, McCrea DA (1995) Effects of stimulation of hindlimb flexor group II afferents during fictive locomotion in the cat. J Physiol 487(Pt 1):211–220

Perreault MC, Shefchyk SJ, Jimenez I, McCrea DA (1999) Depression of muscle and cutaneous afferent-evoked monosynaptic field potentials during fictive locomotion in the cat. J Physiol 521(Pt 3):691–703

Pratt CA, Jordan LM (1987) Ia inhibitory interneurons and Renshaw cells as contributors to the spinal mechanisms of fictive locomotion. J Neurophysiol 57:56–71

Prilutsky BI (2000) Coordination of two- and one-joint muscles: functional consequences and implications for motor control. Motor Control 4:1–44

Prilutsky BI, Klishko AN, Weber DJ, Lemay MA (2015) Computing motion dependent afferent activity during cat locomotion using a forward dynamics musculoskeletal model. In: Prilutsky BI, Edwards DH Jr (eds) Neuromechanical modeling of posture and locomotion. Springer, New York

Prilutsky BI, Maas H, Bulgakova M, Hodson-Tole EF, Gregor RJ (2011) Short-term motor compensations to denervation of feline soleus and lateral gastrocnemius result in preservation of ankle mechanical output during locomotion. Cells Tissues Organs 193:310–324

Prochazka A (1999) Quantifying proprioception. Prog Brain Res 123:133–142

Prochazka A, Gorassini M (1998) Models of ensemble firing of muscle spindle afferents recorded during normal locomotion in cats. J Physiol 507(Pt 1):277–291

Prochazka A, Gillard D, Bennett DJ (1997) Positive force feedback control of muscles. J Neurophysiol 77:3226–3236

Quevedo J, Fedirchuk B, Gosgnach S, McCrea DA (2000) Group I disynaptic excitation of cat hindlimb flexor and bifunctional motoneurones during fictive locomotion. J Physiol 525(Pt 2):549–564

Ross KT, Nichols TR (2009) Heterogenic feedback between hindlimb extensors in the spontaneously locomoting premammillary cat. J Neurophysiol 101:184–197

Rossignol S (1996) Neural control of stereotypic limb movements. In: Rowell LB, Sheperd JT (eds) Handbook of physiology, section 12. Exercise: regulation and integration of multiple systems. Vol 12. American Physiological Society, Oxford, pp 173–216

Rossignol S, Dubuc R, Gossard JP (2006) Dynamic sensorimotor interactions in locomotion. Physiol Rev 86:89–154

Ryall RW (1970) Renshaw cell mediated inhibition of Renshaw cells: patterns of excitation and inhibition from impulses in motor axon collaterals. J Neurophysiol 33:257–270

Rybak IA, Ivashko DG, Prilutsky BI, Lewis MA, Chapin JK (2002) Modeling neural control of locomotion: Integration of reflex circuits with CPG. In: Dorronsoro J (ed) Artificial neural networks. Springer Berlin Heidelberg, pp 99–104

Rybak IA, Shevtsova NA, Lafreniere-Roula M, McCrea DA (2006a) Modelling spinal circuitry involved in locomotor pattern generation: insights from deletions during fictive locomotion. J Physiol 577:617–639

Rybak IA, Stecina K, Shevtsova NA, McCrea DA (2006b) Modelling spinal circuitry involved in locomotor pattern generation: insights from the effects of afferent stimulation. J Physiol 577:641–658

Rybak IA, Shevtsova NA, Kiehn O (2013) Modelling genetic reorganization in the mouse spinal cord affecting left-right coordination during locomotion. J Physiol 591:5491–5508

Sacks RD, Roy RR (1982) Architecture of the hind limb muscles of cats: functional significance. J Morphol 173:185–195

Shevtsova NA, Hamade K, Chakrabarty S, Markin SN, Prilutsky BI, Rybak IA (2015) Modeling the organization of central neural circuits controlling two-joint muscles. In: Prilutsky BI, Edwards DH Jr (eds) Neuromechanical modeling of posture and locomotion. Springer, New York

Spector SA, Gardiner PF, Zernicke RF, Roy RR, Edgerton VR (1980) Muscle architecture and force-velocity characteristics of cat soleus and medial gastrocnemius: implications for motor control. J Neurophysiol 44:951–960

Stecina K, Quevedo J, McCrea DA (2005) Parallel reflex pathways from flexor muscle afferents evoking resetting and flexion enhancement during fictive locomotion and scratch in the cat. J Physiol 569:275–290

Stein RB, Misiaszek JE, Pearson KG (2000) Functional role of muscle reflexes for force generation in the decerebrate walking cat. J Physiol 525(Pt 3):781–791

Taga G (1995a) A model of the neuro-musculo-skeletal system for human locomotion. I. Emergence of basic gait. Biol Cybern 73:97–111

Taga G (1995b) A model of the neuro-musculo-skeletal system for human locomotion. II Real-time adaptability under various constraints. Biol Cybern 73:113–121

Toth TI, Schmidt J, Buschges A, Daun-Gruhn S (2013) A neuro-mechanical model of a single leg joint highlighting the basic physiological role of fast and slow muscle fibres of an insect muscle system. PLoS ONE 8:e78247

Wadden T, Ekeberg O (1998) A neuro-mechanical model of legged locomotion: single leg control. Biol Cybern 79:161–173

Whelan PJ (1996) Control of locomotion in the decerebrate cat. Prog Neurobiol 49:481–515

Whelan PJ, Pearson KG (1997) Comparison of the effects of stimulating extensor group I afferents on cycle period during walking in conscious and decerebrate cats. Exp Brain Res 117:444–452

Windhorst U (1996) On the role of recurrent inhibitory feedback in motor control. Prog Neurobiol 49:517–587

Yakovenko S (2011) Chapter 10-a hierarchical perspective on rhythm generation for locomotor control. Prog Brain Res 188:151–166

Yakovenko S, Gritsenko V, Prochazka A (2004) Contribution of stretch reflexes to locomotor control: a modeling study. Biol Cybern 90:146–155

Zhong G, Shevtsova NA, Rybak IA, Harris-Warrick RM (2012) Neuronal activity in the isolated mouse spinal cord during spontaneous deletions in fictive locomotion: insights into locomotor central pattern generator organization. J Physiol 590:4735–4759